CCT2 defines a highly cisplatin-resistant and poor-prognosis subtype of lung adenocarcinoma

HUAFANG MAO, CHAO SU, XIAOLIANG HAN and GUOXIA WANG

Department of Thoracic Surgery, The Affiliated Hospital of Shaoxing University (Shaoxing Municipal Hospital), Shaoxing, Zhejiang 312000, P.R. China

Received January 22, 2026; Accepted July 29, 2026

DOI: 10.3892/ol.2026.15836

Abstract. Cisplatin-based chemotherapy is a standard treatment for lung adenocarcinoma (LUAD), yet acquired cisplatin resistance remains a marked cause of treatment failure. The molecular mechanisms driving cisplatin resistance in LUAD have not been fully elucidated. The present study integrated bulk transcriptomic data, genomic mutation profiles and single-cell RNA sequencing data to systematically investigate cisplatin resistance in LUAD. Resistance-associated genes were identified through differential expression, survival analysis and database integration. Unsupervised clustering was used to define cisplatin resistance-associated subtypes. Functional characteristics were explored using pathway enrichment, immune infiltration, tumor mutation burden and weighted gene co-expression network analysis. A machine learning framework incorporating 101 algorithms was applied to identify key genes and construct a prognostic model. Single-cell analyses and *in vitro* experiments were performed to validate the biological role of the core gene. Molecular docking and molecular dynamics simulations were conducted to identify potential therapeutic compounds. A total of two molecular subtypes with distinct cisplatin resistance levels and prognostic outcomes were identified. The high-resistance subtype exhibited enhanced cell cycle activity, DNA repair signaling and immune heterogeneity. Machine learning analysis revealed a five-gene signature, with chaperonin-containing TCP1 subunit 2 (CCT2) emerging as a key regulator of cisplatin resistance. Single-cell analyses showed that CCT2 was predominantly enriched in resistant epithelial cell subpopulations. Functional experiments demonstrated that CCT2 knockdown significantly inhibited cell proliferation and enhanced cisplatin sensitivity in LUAD cell lines. A number of candidate compounds targeting CCT2 exhibited stable binding *in silico*. The present findings identified CCT2 as a key mediator of cisplatin resistance in LUAD and provided potential therapeutic strategies to overcome chemotherapy resistance.

Introduction

Lung cancer is the most frequently diagnosed cancer and the leading cause of cancer-related mortality worldwide, with ~2.6 million new cases and 1.9 million mortalities estimated globally in 2024, while lung adenocarcinoma (LUAD) is the most prevalent histological subtype of non-small cell lung cancer (NSCLC) (1-4). Despite notable advances in early diagnosis and the development of targeted therapies and immune checkpoint inhibitors, platinum-based chemotherapy remains an established treatment for patients with advanced or metastatic LUAD who lack actionable driver mutations (5-7). Cisplatin, one of the most widely used platinum agents, exerts its antitumor effects primarily through the induction of DNA cross-linking and subsequent apoptosis (8,9). However, the clinical benefit of cisplatin is frequently compromised by the rapid emergence of acquired resistance, which leads to treatment failure and disease progression (10,11). Cisplatin resistance therefore represents a major clinical challenge and a key barrier to improving long-term survival outcomes in patients with LUAD.

To overcome cisplatin resistance, a number of therapeutic strategies have been explored in recent years. Combination regimens integrating cisplatin with targeted agents, immune checkpoint inhibitors or modulators have shown partial efficacy in delaying resistance and improving response rates (12-16). In

Correspondence to: Dr Guoxia Wang, Department of Thoracic Surgery, The Affiliated Hospital of Shaoxing University (Shaoxing Municipal Hospital), 999 Zhongxing South Road, Yuecheng, Shaoxing, Zhejiang 312000, P.R. China
E-mail: wgx1991@126.com

Abbreviations: LUAD, lung adenocarcinoma; NSCLC, non-small cell lung cancer; TCGA, The Cancer Genome Atlas; ICGC, International Cancer Genome Consortium; GEO, Gene Expression Omnibus; DEGs, differentially expressed genes; GSEA, Gene Set Enrichment Analysis; ssGSEA, single-sample GSEA; GSVA, Gene Set Variation Analysis; IRGSEA, immune-related GSEA; WGCNA, weighted gene co-expression network analysis; PPI, protein-protein interaction; CNV, copy number variation; KEGG, Kyoto Encyclopedia of Genes and Genomes; BP, biological process; TMB: tumor mutational burden; CCT, chaperonin-containing TCP-1; CMAP, connectivity map; MOE, Molecular Operating Environment; RMSD, root mean square deviation

Key words: lung adenocarcinoma, cisplatin resistance, chaperonin-containing TCP-1 subunit 2, single-cell analysis, machine learning

addition, previous studies have demonstrated that the inhibition of DNA damage repair pathways, modulation of oxidative stress responses and targeting of cell cycle regulators may sensitize tumor cells to cisplatin (17-22). Despite this, these approaches often yield heterogeneous clinical responses and may be accompanied by increased toxicity or limited applicability to specific patient subgroups. These limitations highlight the urgent need to identify robust molecular determinants of cisplatin resistance and to develop more precise, mechanism-based therapeutic strategies.

At the molecular level, cisplatin resistance is a multifactorial process that involves alterations in DNA repair capacity, cell cycle regulation, metabolic reprogramming, apoptosis evasion, autophagy and tumor microenvironment remodeling (23-26). Recently, posttranslational modifications have emerged as important regulators of drug resistance (27-29). Among them, protein palmitoylation is a reversible lipid modification that serves a key role in controlling protein stability, subcellular localization and signal transduction (30-32). Accumulating evidence has further suggested that dysregulated palmitoylation contributes to tumor progression and therapeutic resistance by affecting oncogenic signaling pathways (such as the ZDHHC Palmitoyltransferase 20-YTH domain-containing family protein 3-MYC and claudin 4-Notch axes), cellular metabolism and stress responses (33-38). However, the contribution of palmitoylation-associated genes to cisplatin resistance in LUAD, as well as their interactions with tumor heterogeneity and the immune microenvironment, remain largely unexplored.

Recent studies have demonstrated that integrated bioinformatics and machine learning approaches can effectively identify disease-specific biomarkers and characterize immune landscapes across diverse pathological conditions. For example, mitochondrial dysfunction-associated biomarkers identified in liver ischemia-reperfusion injury have been associated with increased neutrophil and activated mast cell infiltration, along with reduced M2 macrophages (39). In addition, in clear cell renal cell carcinoma, an immunogenic cell death-associated prognostic signature effectively predicted overall survival, disease progression, distinct immune infiltration patterns and improved immunotherapy responses in patients at high-risk (40).

Similarly, in hepatocellular carcinoma, a polyamine metabolism-associated prognostic signature showed strong prognostic value and revealed notable differences in immune cell infiltration and immune treatment sensitivity between risk groups (41). These findings further highlight the translational potential of such strategies in precision medicine. The present study systematically investigated cisplatin resistance in LUAD by defining resistance-associated molecular subtypes and identifying key regulatory genes with prognostic and functional relevance. In this study, we aimed to systematically characterize cisplatin resistance heterogeneity in LUAD by integrating multilevel transcriptomic analyses, including bulk and single-cell RNA sequencing approaches. We sought to identify resistance-associated molecular subtypes, discover key molecular determinants underlying cisplatin resistance, and investigate their potential biological relevance through comprehensive bioinformatic analyses and experimental validation. This integrated framework may provide new insights into the molecular mechanisms of cisplatin resistance and facilitate the development of more precise therapeutic strategies for patients with LUAD.

Materials and methods

Data collection. Transcriptomic data of LUAD were obtained from The Cancer Genome Atlas (TCGA) database (https://portal.gdc.cancer.gov), including gene expression profiles and corresponding clinical information. An independent cohort from the International Cancer Genome Consortium (ICGC) database (https://dcc.icgc.org), specifically the ICGC-LUAD-US cohort, was used for external validation of the prognostic model. Cisplatin-resistant transcriptomic data were retrieved from the Gene Expression Omnibus (GEO) database (https://www.ncbi.nlm.nih.gov/geo), specifically dataset GSE213102 (42). Single-cell RNA sequencing (RNA-seq) data were obtained from the GEO dataset GSE229253 (43). All datasets were processed and normalized according to their respective preprocessing pipelines prior to downstream analyses.

Collection of cisplatin resistance gene sets. Cisplatin resistance-associated genes were retrieved from the GeneCards database (https://www.genecards.org/). The keyword 'cisplatin-resistant' was used to perform a systematic search and genes with relevance scores provided by GeneCards were extracted. The resulting gene list was downloaded and curated to obtain a cisplatin resistance gene set for subsequent analyses.

Unsupervised clustering analysis. Unsupervised clustering was performed using the 'ConsensusClusterPlus' R package (44) (version 1.68.0) based on the expression profiles of treatment group samples from the TCGA-LUAD cohort. The expression matrix was subjected to consensus clustering with the k-means algorithm and Euclidean distance. Clustering stability was evaluated across 50 resampling iterations, with 80% of the samples and all the features randomly selected in each iteration. The optimal number of clusters was determined by inspecting the cumulative distribution function curves and consensus heatmaps, supplemented by item-consensus and cluster-consensus scores derived from the integrated consensus likelihood analysis (44). The samples were subsequently assigned to their respective consensus clusters and the resulting subtype information was exported for downstream analyses.

Single-sample Gene Set Enrichment Analysis (ssGSEA). To quantify pathway activity at the individual sample level, ssGSEA was performed using gene expression data from the TCGA-LUAD cohort. Gene expression matrices were preprocessed by converting expression values to numeric formats, removing duplicated genes through average expression consolidation and genes with low overall expression were filtered. Curated gene sets were imported from a gene matrix transposed (GMT) file using the GSEABase R package (version 1.70.0; DOI, 10.18129/B9.bioc.GSEABase). ssGSEA scores for each gene set were then computed using the 'ssgsea' method and Gaussian kernel estimation and the genes were

ranked by absolute expression. To facilitate cross-sample comparison, raw ssGSEA enrichment scores were normalized using a min-max scaling transformation. The resulting normalized enrichment matrix was used for subsequent statistical analyses.

GSEA. GSEA was performed using gene expression data from the TCGA-LUAD cohort to identify pathway differences between the two molecular subgroups. The analysis was conducted using GSEA software (https://www.gsea-msigdb.org/gsea/index.jsp) with the Kyoto Encyclopedia of Genes and Genomes (KEGG) and REACTOME gene sets downloaded from the Molecular Signatures Database (MSigDB; https://www.gsea-msigdb.org/gsea/msigdb/). Genes were ranked according to the signal-to-noise ratio between the two subgroups and enrichment was assessed using 1,000 permutations. Pathways with a nominal $P<0.05$ were considered to be significantly enriched.

Cell-type identification by estimating relative subsets of RNA transcripts (CIBERSORT) immune infiltration analysis. Immune cell infiltration was quantified using the CIBERSORT algorithm (45) based on bulk RNA sequencing data from the TCGA-LUAD cohort, which applied ν-support vector regression (ν-SVR) to deconvolute the relative proportions of 22 immune cell subsets. The LM22 leukocyte signature matrix was used as the reference gene expression profile and the mixed expression matrix was quantile-normalized prior to deconvolution. To improve robustness, CIBERSORT fitted multiple ν-SVR models with different ν parameters and selected the model with the minimal root-mean-square error. For each sample, CIBERSORT returned the estimated immune cell fractions along with correlation coefficients and root-mean-square error values reflecting deconvolution accuracy. Permutation testing was performed when needed to compute empirical P-values and samples with $P<0.05$ were considered to have reliable immune infiltration estimates.

Tumor mutational burden (TMB) analysis. Tumor mutation burden analysis was performed using somatic mutation data downloaded from TCGA-LUAD cohort. Masked somatic mutation (MAF) files were retrieved from the National Cancer Institute Genomic Data Commons database (https://portal.gdc.cancer.gov/) and merged to generate a unified mutation profile. The MAF data were processed and annotated using the 'maftools' R package (version 2.18.0) (46) and TMB was calculated as the total number of non-synonymous somatic mutations per megabase for each sample. To compare mutational landscapes between molecular subgroups, sample identifiers were matched to cluster assignments and subgroup-specific MAF objects (for example, C1 and C2) were generated. Mutation profiles were visualized using the oncoplots function implemented in maftools, which displays the most frequently mutated genes across molecular subgroups.

Differential gene expression analysis. Differential expression analysis was performed on TCGA-LUAD transcriptomic data using the 'limma' R package (version 3.58.1) (47). Expression matrices were $\log_2$-transformed prior to analysis. A design matrix was constructed based on control and treatment groups, and linear models were fitted using the lmFit function implemented in limma, followed by empirical Bayes moderation. Differentially expressed genes were identified using a contrast comparison between the C1 and C2 groups. In parallel, the GSE213102 dataset, which includes cisplatin-resistant and cisplatin-sensitive cell lines, was analyzed using the same 'limma'-based differential expression pipeline to identify resistance-associated genes.

Weighted gene coexpression network analysis (WGCNA). WGCNA was performed using the 'WGCNA' R package (version 1.73) (48) based on gene expression data from the TCGA-LUAD cohort. After low-variance genes were removed, the top 25% of the most variable genes were selected for network construction. The sample quality was assessed by hierarchical clustering and outlier samples were excluded. Soft-thresholding power was determined using the scale-free topology criterion (48) and an adjacency matrix was constructed and transformed into a topological overlap matrix (TOM). Genes were clustered on the basis of TOM dissimilarity and coexpression modules were identified using dynamic tree cutting. Module eigengenes were calculated and correlated with cluster membership (C1 and C2 subgroups) to identify trait-associated modules. Gene significance and module membership were computed to screen for hub genes within key modules.

Functional enrichment analysis. Gene Ontology (GO) (49) and KEGG (50) enrichment analyses were performed using the 'clusterProfiler' R package (version 4.10.1) (51). Gene sets were first converted from gene symbols to Entrez IDs using the org.Hs.eg.db annotation database (https://bioconductor.org/packages/org.Hs.eg.db/) and genes without valid Entrez IDs were removed. GO enrichment analysis [biological processes (BPs), cellular components and molecular functions] and KEGG pathway enrichment analysis were subsequently performed, with the organism set to 'hsa'. Enriched terms were filtered using $P<0.05$ as the significance threshold. The results were visualized using the 'enrichplot' (version 1.22.0) (https://bioconductor.org/packages/enrichplot/) and 'ggplot2' R packages (version 3.5.0) (https://cran.r-project.org/package=ggplot2).

Protein-protein interaction (PPI) network analysis. Gene set were imported into the Search Tool for the Retrieval of Interacting Genes/Proteins (STRING) database (https://string-db.org/) to construct a protein-protein interaction network using a confidence score threshold of 0.4. The resulting interaction network was downloaded and further visualized in Cytoscape (https://cytoscape.org/). Topological parameters were calculated and key hub genes were identified using the built-in 'NetworkAnalyzer' tool or the 'CytoHubba' plugin.

Machine learning-based feature selection and modeling. To construct a robust prognostic signature, an integrative machine learning framework encompassing 101 different algorithmic combinations was employed. Gene expression data from the TCGA served as the training set, while ICGC data were used for independent validation. Candidate genes were preselected

based on univariate Cox regression analysis (P<0.05). The machine learning framework incorporated 10 algorithms, including Random Survival Forest (RSF), Elastic Net (Enet), Stepwise Cox regression (StepCox), CoxBoost, partial least squares regression for Cox (plsRcox), supervised principal components (superpc), gradient boosting machine (GBM), survival support vector machine (survival-SVM), Ridge regression and Lasso regression, as well as their specified pairwise combinations, resulting in 101 candidate models. Model development and selection were performed using ML.Dev.Prog. The Sig pipeline in R (with the following packages: 'GSEABase' (version 1.70.0; DOI, 10.18129/B9.bioc.GSEABase), Gene Set Variation Analysis ('GSVA'; version 1.50.5) (52), 'cancerclass' (version 1.46.0) (53), 'mixOmics' (version 6.26.0) (54), 'sparrow' (version 1.8.5; DOI, 10.18129/B9.bioc.sparrow), 'sva' (version 3.50.0) (55), 'ComplexHeatmap' (version 2.18.0) (56), 'CoxBoost' (version 1.5) (57), 'fastAdaboost' [version 1.0.0; https://github.com/souravc83/fastAdaboost) and 'Mime1' (version 0.0.0.9) (58)] was used. Model performance was evaluated by the concordance index (C-index) in both the training and validation cohorts. Visualization of C-index distributions across all the models was performed using the 'cindex_dis_all' function, with the top-performing models further selected for downstream analyses.

Single-cell RNA-seq analysis. Single-cell RNA-seq data from the GSE229253 dataset were processed using the 'Seurat' R package (version 5.3) (59). Quality control was performed by calculating the mitochondrial gene ratio (percent.mt) and hemoglobin gene ratio (percent.HB), followed by filtering cells with nFeature_RNA >200, nFeature_RNA <7,500, nCount_RNA >1,000 and percent.mt <20%. After normalization, highly variable genes were identified and scaling and dimensionality reduction were conducted using principal component analysis. Batch effects were corrected using the Harmony algorithm. Clustering was carried out with 'FindNeighbors' and 'FindClusters' and the results were visualized using Uniform Manifold Approximation and Projection. Cluster-specific marker genes were identified using 'FindAllMarkers' with the Wilcoxon test. Cell-type annotation was performed with 'SingleR' (version 2.4.1) (60) using the Human Primary Cell Atlas as the reference and further validated by cross-referencing significant marker genes with the CellMarker database (http://bio-bigdata.hrbmu.edu.cn/CellMarker/).

Cell-cell communication analysis. Cell-cell communication was analyzed using the 'CellChat' R package (version 1.6.1) (61). Normalized count matrices and cell-type annotations were used to construct the CellChat object and the human ligand-receptor database was used to identify overexpressed signaling genes and ligand-receptor pairs. The communication probabilities and pathway-level interactions were computed, filtered and visualized to characterize the intercellular signaling networks.

Single-cell GSEA. To evaluate the activity of a custom cisplatin resistance-associated gene set at the single-cell level, tumor epithelial cells were extracted from the GSE229253 single-cell RNA-sequencing dataset and analyzed using the immune-related GSEA ('irGSEA') R package (version 3.3.2; https://github.com/chuiqin/irGSEA). The custom gene set was generated from cisplatin resistance-associated genes identified in the present study and converted into GMT format for enrichment analysis. The expression matrix was normalized; highly variable genes were identified and data were scaled using the 'Seurat' R package. Gene set activity in individual cells was calculated using six scoring methods implemented in 'irGSEA', including AUCell, UCell, Variance-adjusted Mahalanobis, Single-Cell Signature Explorer, ssGSEA and singscore. The resulting enrichment scores are visualized as violin plots to compare the activity of the custom cisplatin resistance-associated gene set across different tumor epithelial cell subpopulations.

Copy number variation (CNV) analysis. Single-cell CNVs were inferred using the 'inferCNV' R package (version 1.18.1) (62). Raw unique molecular identifier count matrices were extracted from the Seurat object and gene genomic coordinates were annotated and ordered using the AnnoProbe R package (version 0.1.7; https://github.com/shengqh/AnnoProbe), excluding genes on chromosome (chr)-M, chrX and chrY. Normal cells were used as the reference group. The inferCNV object was constructed from the expression matrix, cell annotations and gene order file and CNV inference was performed with a cut-off of 0.1, denoising enabled and hierarchical clustering using the ward.D2 method. The resulting CNV profiles were used to identify malignant epithelial cell populations.

Cell culture. Human LUAD cell line A549 and NSCLC cell line H1299 were obtained from the American Type Culture Collection. A549 cells are derived from human LUAD epithelial cells, while H1299 cells are derived from human non-small cell lung carcinoma lacking p53 expression. A549 cells were cultured in F-12K medium (cat. no. PM150910; Procell Life Science & Technology Co., Ltd.) and H1299 cells were maintained in RPMI-1640 medium (cat. no. PM150110; Procell Life Science & Technology Co., Ltd.), both supplemented with 10% FBS (cat. no. FSD500; Shanghai ExCell Biology, Inc.) and 1% penicillin-streptomycin. All cells were cultured at 37˚C in a humidified incubator with 5% CO_2.

Gene knockdown assays. Gene knockdown was performed using short hairpin (sh)-RNA expression vectors targeting human CCT2. A total of two shRNA sequences targeting human CCT2 were newly designed and cloned into the pGPU6-GFP-Neo vector backbone by Shanghai GenePharma Co., Ltd. A non-targeting shRNA vector was used as the negative control. Cells were seeded in 6-well plates at 50-60% confluence and transfected with 2.5 μg shRNA plasmid per well using Hieff Trans™ Booster DNA/RNA Transfection Reagent (Lipo3000 alternative; cat. no. 40801ES04; Shanghai Yeasen Biotechnology Co., Ltd.) according to the manufacturer's instructions. After 48-72 h, the knockdown efficiency was assessed by reverse transcription-quantitative PCR (RT-qPCR) and western blotting. For RT-qPCR, total RNA was extracted using TRNzol Universal Reagent (cat. no. DP424; Tiangen Biotech Co., Ltd.), reverse transcribed according to the manufacturer's instructions with a Hifair® III 1st Strand cDNA Synthesis SuperMix for qPCR (gDNA digester plus;

cat. no. 11141ES10; Shanghai Yeasen Biotechnology Co., Ltd.) and amplified using Hieff UNICON™ Universal Blue qPCR Master Mix (SYBR; cat. no. 11184ES03; Shanghai Yeasen Biotechnology Co., Ltd.). qPCR amplification was performed on a QuantStudio™ 3 Real-Time PCR System with an initial denaturation at 95˚C for 30 sec, followed by 40 cycles of 95˚C for 3 sec and 60˚C for 20 sec. Relative gene expression was normalized to GAPDH and calculated using the $2^{-\Delta\Delta Cq}$ method (63). All shRNA and primer sequences are listed in the Table SI.

Western blotting. Total protein was extracted from A549 and H1299 cells using RIPA lysis buffer (Yeasen Biotechnology Co., Ltd.; cat. no. 20115ES60) and quantified using a BCA assay. Equal amounts of protein (20 μg per lane) were separated by 12% SDS-PAGE and transferred onto PVDF membranes. After blocking with 5% skim milk at room temperature for 2 h, membranes were incubated overnight at 4˚C with primary antibodies against CCT2 (cat. no. HA722240; 1:1,000; HUABIO) and GAPDH (cat. no. ET1601-4; 1:50,000; HUABIO), diluted in 5% BSA. After washing, membranes were incubated with HRP-conjugated secondary antibodies (cat. no. HA1001; 1:50,000; HUABIO) at room temperature for 1 h. Protein bands were visualized using an enhanced chemiluminescence system (Enhanced Chemiluminescence Detection Kit; Yeasen Biotechnology Co., Ltd.; cat. no. 36208ES) and quantified using ImageJ software (version 1.8.0; National Institutes of Health).

Cell proliferation assay. Cell proliferation was evaluated using a Cell Counting Kit-8 (CCK-8; cat. no. AC11L054; Heyuan Liji (Shanghai) Biotechnology Co., Ltd.) assay. Cells were seeded in 96-well plates at $2x10^3$ cells per well and incubated at 37˚C for the indicated durations. At each time point, 10 μl CCK-8 solution was added to each well and incubated for 2 h. The absorbance at 450 nm was measured using a microplate reader. All experiments were performed in triplicate.

Cisplatin treatment and cell viability assay. A549 and H1299 cells were first transfected with shRNA expression vectors targeting CCT2 or control shRNA vectors. After transfection, cells were treated with cisplatin (cat. no. P4394; Sigma-Aldrich; Merck KGaA) at final concentrations of 20 μM for A549 cells and 15 μM for H1299 cells at 37˚C for 48 h. Cells were then incubated for 48 h at 37˚C in a humidified atmosphere with 5% CO_2. A total of four experimental groups were included: i) Control; ii) sh-CCT2; iii) cisplatin alone and; iv) cisplatin combined with sh-CCT2. After treatment, cell viability was assessed using the CCK-8 assay according to the manufacturer's instructions.

Molecular docking and molecular dynamics simulation. Molecular docking of CCT2 was performed using the Molecular Operating Environment (MOE; https://www.chemcomp.com). The crystal structure of human CCT2 was prepared by removing water molecules, adding hydrogens, optimizing protonation states and minimizing the protein with the AMBER10:EHT force field. Natural-product ligands were energy-minimized and docked into the predicted binding pocket using the Triangle Matcher placement method (64) and London dG scoring, followed by refinement with Generalized Born Volume Integral/Weighted Surface Area (GBVI/WSA) dG scoring function to obtain the optimal binding poses. The top docking complexes were subsequently subjected to molecular dynamics simulations using GROMACS (https://www.gromacs.org). Protein topologies were generated with the AMBER ff14SB force field and ligand parameters with General Amber Force Field (GAFF). Each complex was placed in a Transferable Intermolecular Potential 3-Point (TIP3P) water box with 0.15 M sodium chloride, energy-minimized, equilibrated under NVT and NPT conditions and simulated for 100 ns at 310 K and 1 bar. Trajectories were analyzed for RMSD, radius of gyration and solvent accessible surface area to evaluate the dynamic behavior and binding stability of each ligand-CCT2 complex.

Statistical analysis. Statistical analyses were performed using GraphPad Prism (version 10.0; Dotmatics). Data are presented as the mean ± SD from at least three independent biological replicates. Comparisons among multiple groups were performed using one-way ANOVA tests followed by Dunnett's or Tukey's multiple comparisons test, as appropriate. For experiments involving two independent variables, statistical significance was determined using two-way ANOVA tests followed by Šidák's multiple comparisons test. $P<0.05$ was considered to indicate a statistically significant difference.

Results

Identification of cisplatin resistance-associated gene signatures in LUAD. First, the transcriptome data of LUAD from the TCGA-LUAD dataset was downloaded, which included 541 tumor samples and 59 adjacent normal lung tissue samples. Differential expression analysis [$\log_2$ fold change (FC) >1; $P<0.05$] revealed 3,234 differentially expressed genes (DEGs), among which 1,229 were upregulated and 2,005 were downregulated in tumor tissues (Fig. 1A). To further identify cisplatin resistance-associated genes, the GSE213102 dataset was retrieved from the GEO database, which contains the transcriptomic profiles of cisplatin-resistant cell lines (A549, H1299, 3B1A and H1573). GEO2R analysis with the same thresholds yielded 1,976 shared DEGs across all the resistant cell lines (Fig. 1B). Univariate Cox regression was then performed to screen prognostic genes among these candidates and obtained cisplatin resistance-associated genes from the GeneCards database. The intersection of upregulated genes, prognostic risk genes, GeneCards-derived cisplatin resistance genes and cisplatin resistance-associated DEGs in LUAD resulted in the identification of a final set of nine cisplatin resistance-associated genes (Fig. 1C). Gene correlation analysis using GeneMANIA (https://genemania.org/) revealed extensive coexpression, physical interactions and colocalization among these genes, which were enriched primarily in BPs such as 'cell cycle G_2/M phase transition', 'chromosome separation' and 'regulation of nuclear division' (Fig. 1D). Unsupervised consensus clustering based on these nine genes revealed two robust molecular subtypes, designated C1 and C2 (Fig. 1E). ssGSEA demonstrated that the cisplatin resistance score was significantly greater in the C1 subtype compared with the C2 subtype (Fig. 1F). Survival analysis further

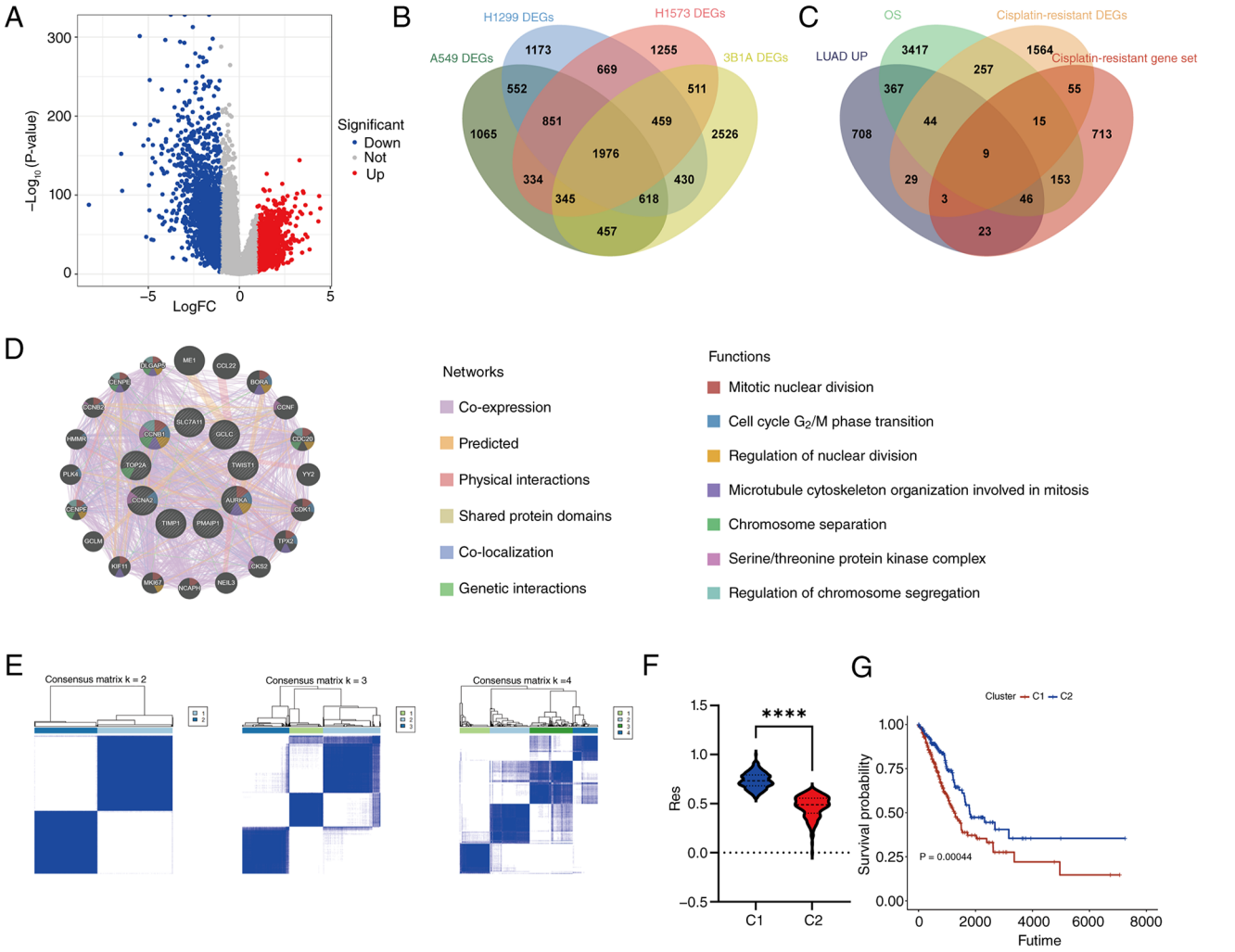

Figure 1. Identification of cisplatin resistance-associated gene signatures and molecular subtypes in LUAD. (A) DEGs between LUAD tumor and normal tissues in The Cancer Genome Atlas cohort. (B) Venn diagram showing the overlap of DEGs among cisplatin-resistant cell lines from the GSE213102 dataset. (C) Venn diagram illustrating the intersection of upregulated genes in LUAD, prognostic risk genes, GeneCards-derived cisplatin resistance genes and cisplatin resistance-associated DEGs, yielding nine candidate genes. (D) GeneMANIA network depicting coexpression and functional interactions among the nine cisplatin resistance-associated genes. (E) Consensus clustering of LUAD samples based on the nine-gene signature, defining two molecular subtypes (C1 and C2). (F) Comparison of single sample Gene Set Enrichment Analysis-derived cisplatin resistance scores between the two subtypes. ****P<0.0001. (G) Kaplan-Meier OS analysis of patients stratified by C1 and C2 subtypes. LUAD, lung adenocarcinoma; DEGs, differentially expressed genes; OS, overall survival; FC, fold change; Up, upregulated; Down, downregulated; Res, resistance.

revealed that patients in the C1 cluster exhibited significantly worse overall survival compared with those in the C2 cluster (log-rank test, P<0.001; Fig. 1G).

Genomic and pathway characteristics of cisplatin-resistance subtypes. To elucidate the differences in gene expression between the two subtypes, TMB analysis was first performed. The highly mutated genes included CUB and sushi multiple domains 3 (CSMD3), erythrocytic spectrin α 1 and xin actin binding repeat containing 2 (Fig. 2A). Notably, compared with the C2 subtype, the C1 subtype exhibited significantly higher mutation frequencies for TP53, titin and CSMD3 (Fig. 2B). The present study subsequently investigated differences in pathway activity between subtypes using GSEA. KEGG-based GSEA revealed that 'KEGG cell cycle', 'KEGG p53 signaling pathway' and 'KEGG mismatch repair' were markedly enriched in the C1 subtype (Fig. 2C). Consistent with these findings, a reactome GSEA revealed significant activation of 'REACTOME DNA repair', 'REACTOME transcriptional regulation by TP53' and 'REACTOME Mitotic G_2/M phases' in the C1 subtype (Fig. 2D). These findings suggested that enhanced genomic instability and checkpoint activation were key molecular hallmarks of the high-resistance C1 cluster.

Immune landscape differences between cisplatin-resistance subtypes. Immunological heterogeneity between the two cisplatin resistance subtypes was first characterized by comparing the expression levels of immune checkpoint-associated genes. The majority of immune checkpoint-associated genes, including glutamate-cysteine ligase catalytic subunit, twist family BHLH transcription factor 1 and phorbol-12-myristate-13-acetate-induced protein 1, were significantly upregulated in the C1 subtype relative to the C2 subtype (Fig. 3A). Immune cell infiltration was then assessed using the CIBERSORT algorithm. A number of immune cell populations, such as naïve B cells, plasma cells and resting CD4 memory T cells, were found to

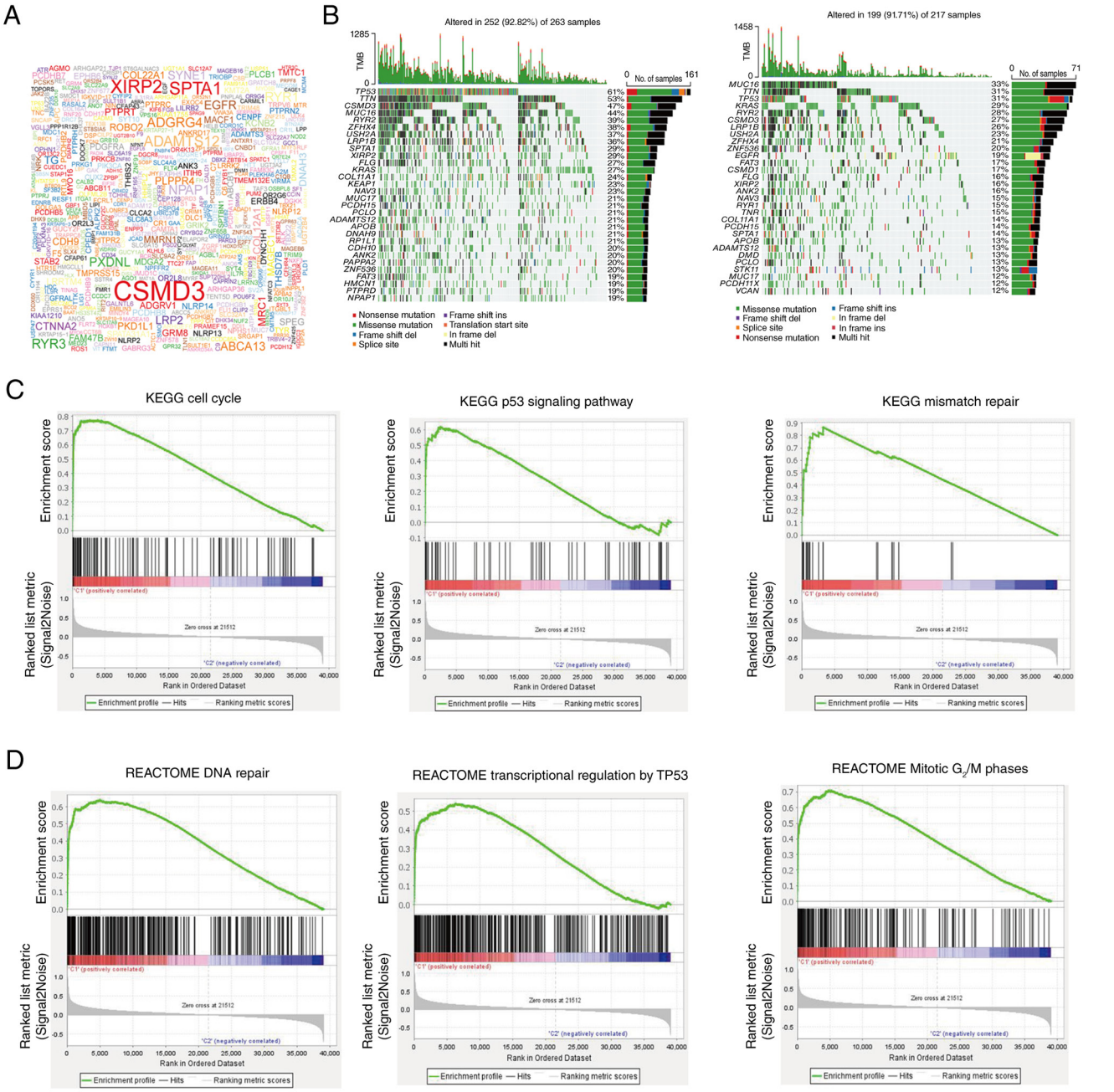

Figure 2. Genomic alterations and pathway enrichment associated with cisplatin resistance subtypes. (A) Somatic mutation landscape and frequently mutated genes in patients with lung adenocarcinoma. (B) Comparison of mutation frequencies of representative genes between the C1 and C2 subtypes. (C) KEGG-based GSEA showing enrichment of cell cycle-, p53 signaling- and mismatch repair-associated pathways in the C1 subtype. (D) Reactome-based GSEA indicating the activation of DNA repair, TP53 regulatory signaling and G_2/M checkpoint pathways in the C1 subtype. KEGG, Kyoto Encyclopedia of Genes and Genomes; GSEA, Gene Set Enrichment Analysis.

be more abundant in the C2 subtype, whereas CD8 T cells were significantly more abundant in the C1 subtype (Fig. 3B). Numerous computational algorithms were subsequently applied to evaluate the correlation between immune infiltration patterns and cisplatin resistance scores. The resistance score was found to be positively correlated with that of resting natural killer cells and follicular helper T cells, indicating an association between the immunological activation state and the cisplatin resistance phenotype (Fig. 3C).

Integrated molecular profiling identifies key pathways and hub genes associated with cisplatin resistance. To investigate the molecular disparities between the two subtypes, differential expression analysis was performed ($\log_2$ FC >0.5; P<0.05) to identify 2,375 DEGs, including 1,224 upregulated genes and 1,151 downregulated genes, in the C2 relative to C1 subtype (Fig. 4A). WGCNA was then conducted, with a soft-thresholding power of 3 (Fig. 4B), resulting in a number of coexpression modules (Fig. 4C). Module-trait correlation analysis revealed numerous clinically relevant modules (Fig. 4D), which were selected for downstream analyses. Given the key role of protein palmitoylation in chemoresistance, palmitoylation-associated genes were incorporated into the analysis. An intersection of DEGs, WGCNA-derived module

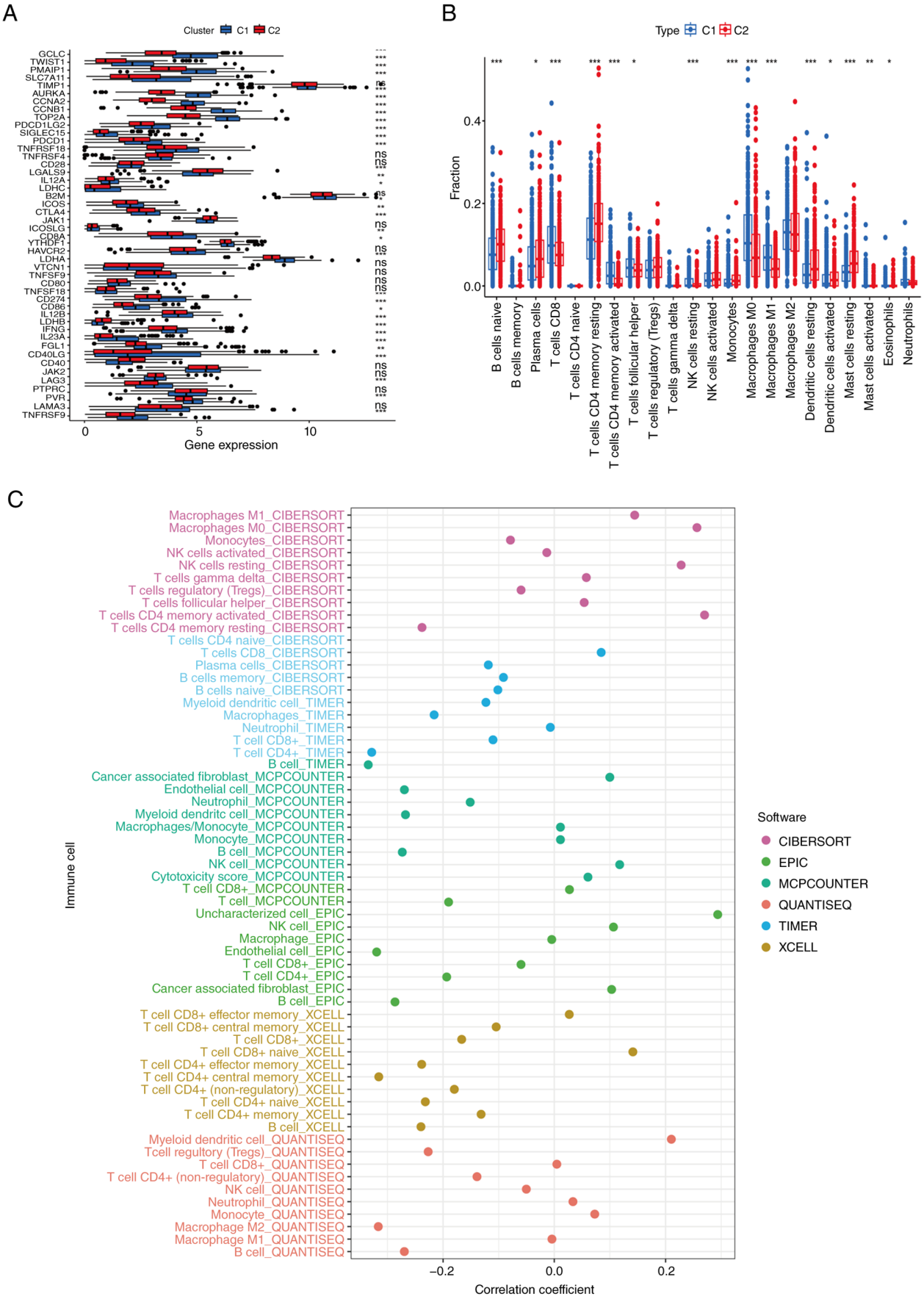

Figure 3. Differences in the immune landscape between cisplatin-resistant subtypes. (A) Differential expression of immune checkpoint-associated genes between the C1 and C2 subtypes. (B) Comparison of immune cell infiltration levels estimated by the CIBERSORT algorithm between the two subtypes. (C) Correlation analysis between immune cell infiltration patterns and cisplatin resistance scores. *P<0.05, **P<0.01, ***P<0.001. ns, not significant; CIBERSORT, Cell-type Identification by Estimating Relative Subsets of RNA Transcripts; MCPCOUNTER, Microenvironment Cell Populations-counter; TIMER, Tumor Immune Estimation Resource.

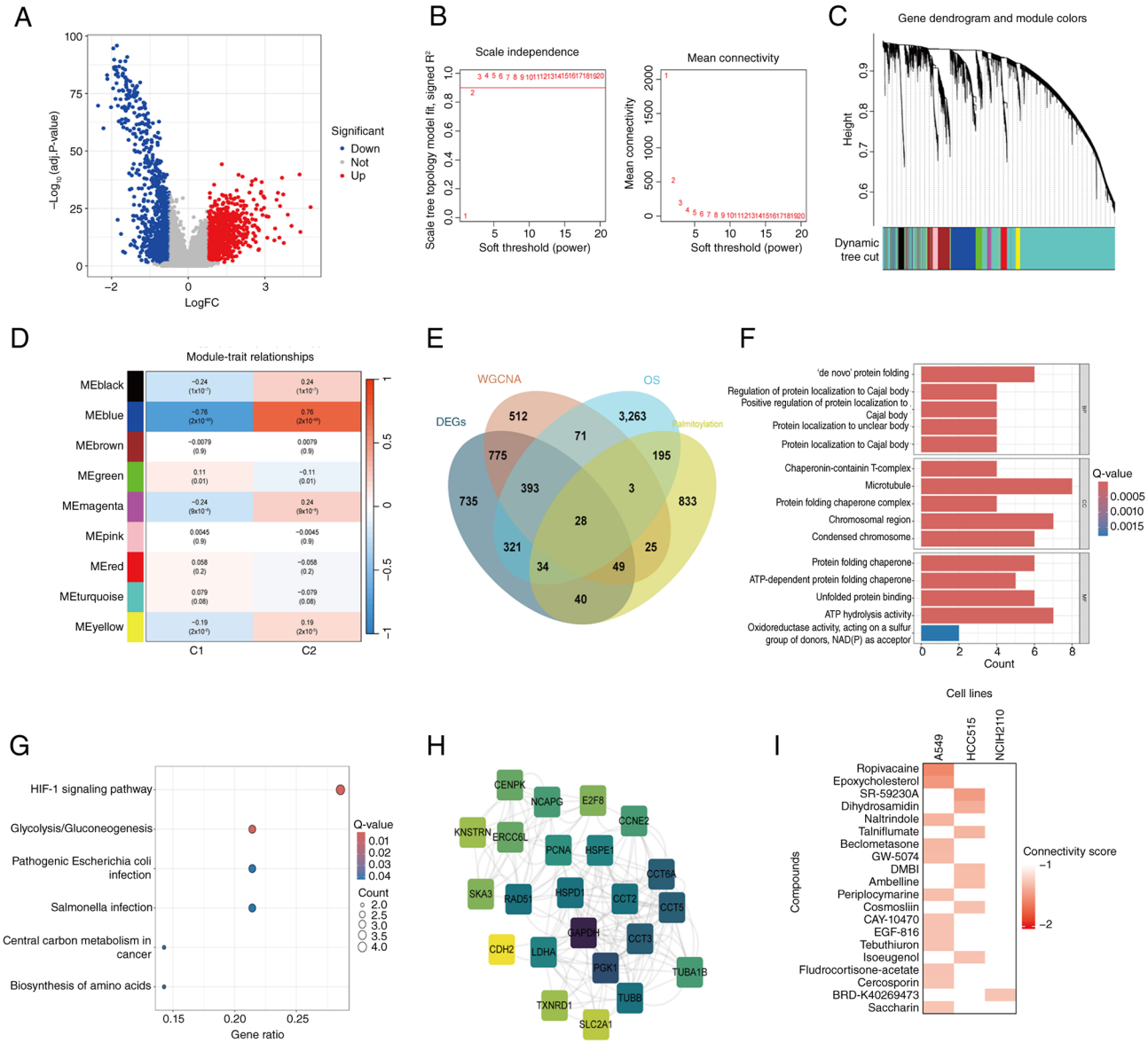

Figure 4. Integrated molecular profiling and identification of key pathways and hub genes associated with cisplatin resistance. (A) Volcano plot of genes differentially expressed between the C1 and C2 subtypes. (B) Determination of the soft-thresholding power in WGCNA. (C) Gene coexpression modules identified by WGCNA. (D) Heatmap showing correlations between gene modules and clinical traits. (E) Venn diagram illustrating the overlap among differentially expressed genes, WGCNA module genes, prognostic genes and palmitoylation-associated genes. (F) Gene Ontology enrichment analysis of the intersecting genes. (G) Kyoto Encyclopedia of Genes and Genomes pathway enrichment analysis of the intersecting genes. (H) Protein-protein interaction network highlighting hub genes identified from the Search Tool for the Retrieval of Interacting Genes/Proteins database. (I) Connectivity Map-based prediction of potential therapeutic compounds targeting the hub genes. WGCNA, Weighted Gene Coexpression Network Analysis; adj., adjusted; FC, fold change; OS, overall survival; ME, Module Eigengene; Up, upregulated; Down, downregulated.

genes, prognostic risk genes and palmitoylation-associated genes yielded 28 shared genes (Fig. 4E). To elucidate the biological functions associated with these genes, GO and KEGG enrichment analyses were performed. GO enrichment revealed involvement in '*de novo* protein folding', 'regulation of protein localization to Cajal body', 'chaperonin-containing T-complex' assembly, 'microtubule' and 'protein folding chaperone' activity (Fig. 4F). KEGG analysis revealed significant enrichment of the 'HIF-1 signaling pathway' and 'glycolysis/gluconeogenesis' (Fig. 4G). PPI analysis using the STRING database revealed GAPDH, CCT2 and CCT3 as central hub genes within the network (Fig. 4H). Finally, CMAP (https://clue.io/cmap) analysis identified several compounds with negative or low connectivity scores, including ropivacaine, epoxycholesterol, naltrindole and beclometasone in A549 cells; SR-59230A, dihydrosamidin, talniflumate, GW-5074, DMBI, cosmosiin and isoeugenol in HCC515 cells; and BRD-K40269473 in NCI-H2110 cells (Fig. 4I).

Identification of key cisplatin-resistance genes using an integrated 101-algorithm machine learning framework. A total of 101 machine learning algorithms were integrated to refine the expression of cisplatin resistance-associated core genes. The TCGA cohort was used for model training and the ICGC cohort was used for external validation. The performance heatmaps of all the algorithmic models are presented in Fig. 5A. Among

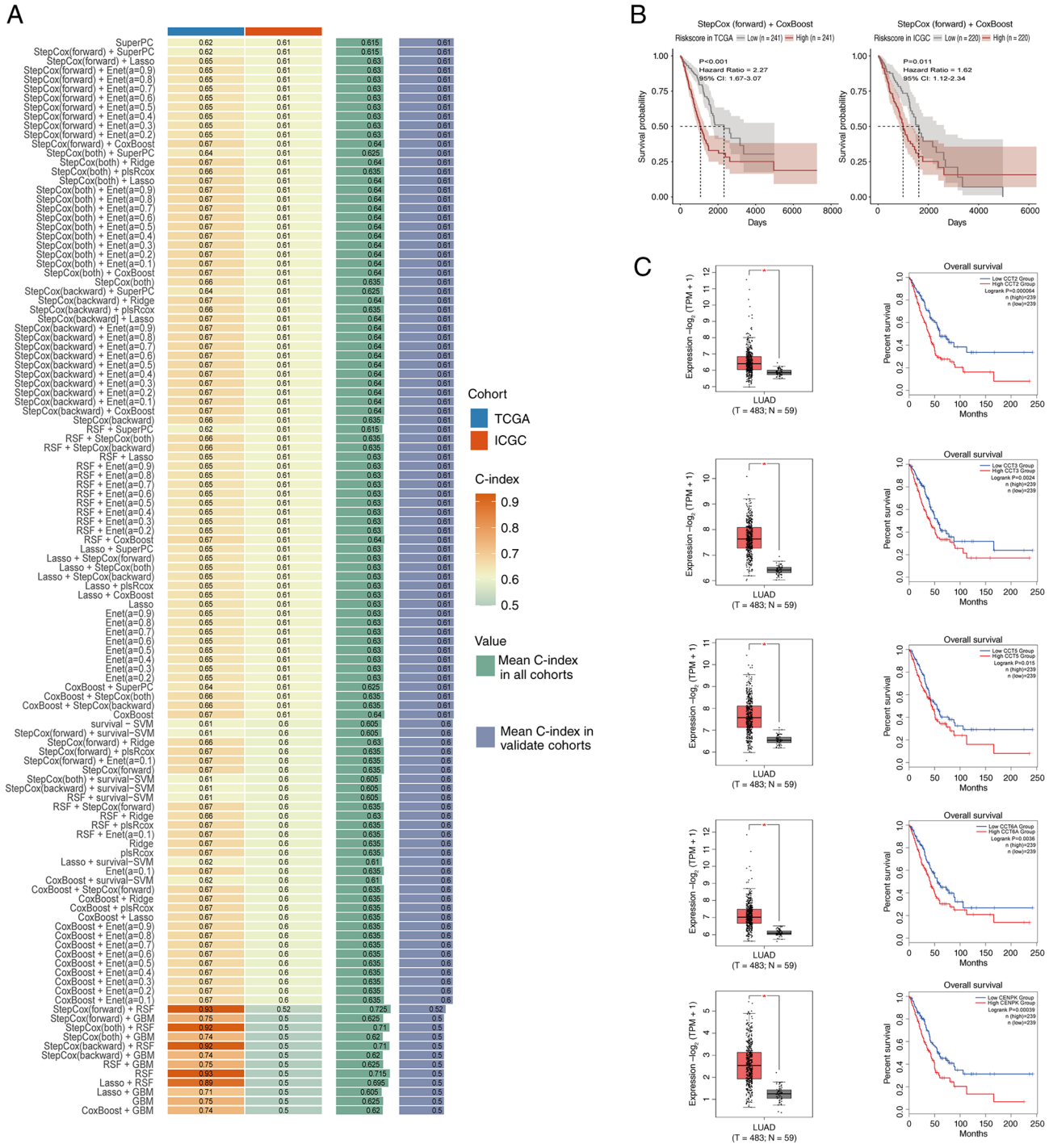

Figure 5. Identification of key cisplatin resistance genes using an integrated 101-algorithm machine learning framework. (A) Heatmap showing the predictive performance of 101 integrated machine learning models in the TCGA training cohort with external validation in the ICGC cohort. (B) Kaplan-Meier survival curves based on risk scores derived from the optimal StepCox (forward) + CoxBoost model in the training and validation datasets. (C) Expression patterns and prognostic significance of the five-gene signature (CCT2, CCT3, CCT5, CCT6A and CENPK) in LUAD. *P<0.05. TCGA, The Cancer Genome Atlas; TPM, transcripts per million; LUAD, lung adenocarcinoma; ICGC, International Cancer Genome Consortium; CCT, chaperonin-containing TCP-1; CENPK, centromere protein K.

all combinations, the StepCox (forward) + CoxBoost model demonstrated the highest predictive accuracy. Survival curves generated from both the training and validation datasets, on the basis of the model-derived risk scores, consistently revealed significant prognostic stratification (Fig. 5B). This optimized model identified five key genes, CCT2, CCT3, CCT5, CCT6A and centromere protein K (CENPK), as the most robust predictors. All five genes were markedly upregulated in LUAD tissues compared with normal lung tissues and patients with high expression of these genes exhibited significantly poorer overall survival compared with those with low expression levels (Fig. 5C). These findings suggested that the five-gene signature served a key role in mediating cisplatin resistance and may serve as a potent biomarker panel for risk assessment.

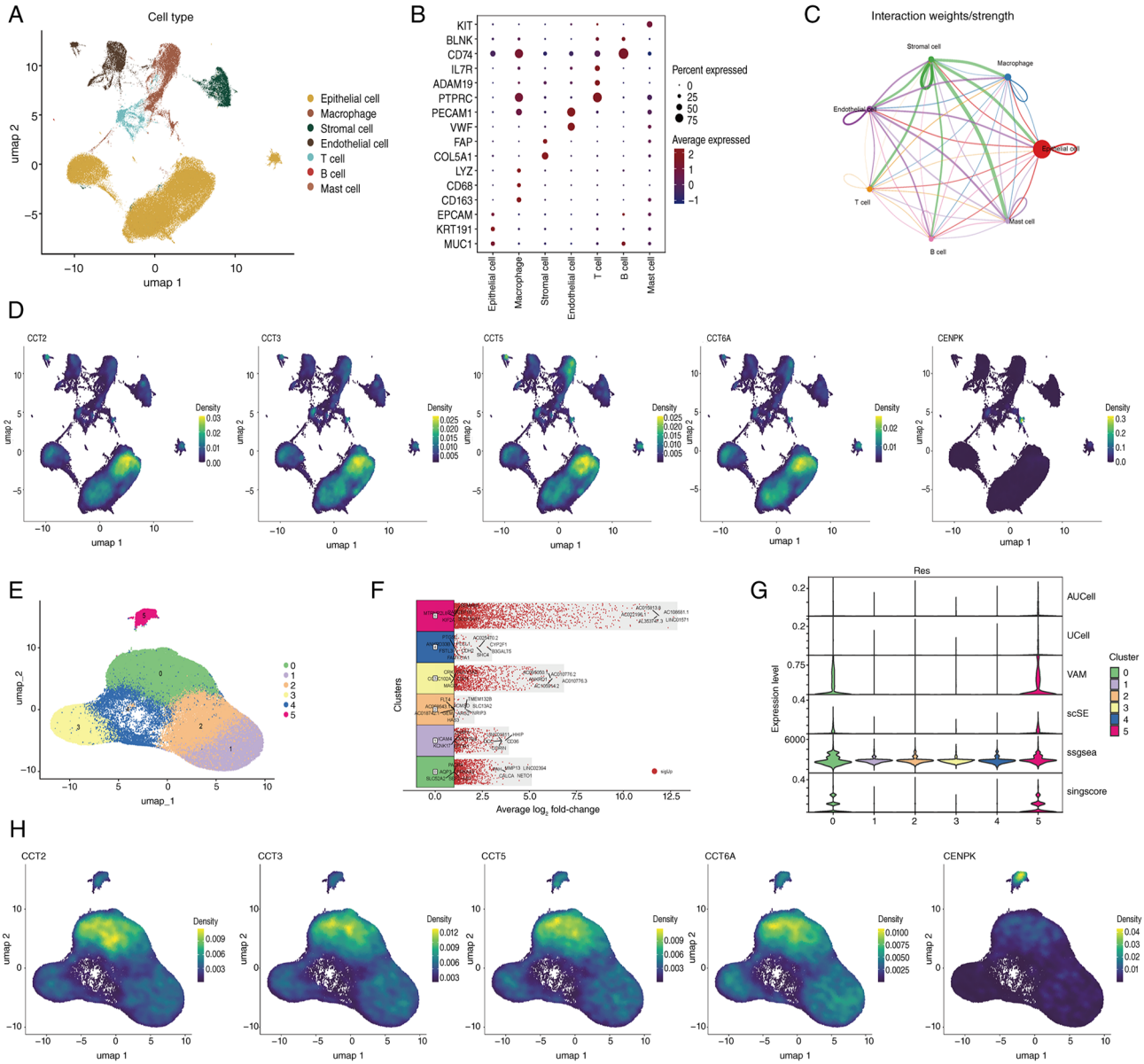

Figure 6. Single-cell transcriptomic profiling revealed enrichment of cisplatin resistance-associated core genes in epithelial cells. (A) UMAP visualization of key cell populations in lung cancer single cell RNA-sequencing data (GSE229253). (B) Canonical marker gene expression for annotated cell types. (C) Cell-cell communication networks inferred by CellChat. (D) Distribution of core gene expression across key cell populations. (E) UMAP of epithelial cell subclusters. (F) Marker gene signatures defining epithelial cell subpopulations. (G) Immune-related Gene Set Enrichment Analysis-based enrichment of cisplatin resistance gene signatures across epithelial subclusters. (H) Expression patterns of the five core genes across epithelial subclusters, highlighting enrichment in cisplatin-resistant populations. CCT, chaperonin-containing TCP-1; CENPK, centromere protein K; UMAP, Uniform Manifold Approximation and Projection; VAM, Variance-adjusted Mahalanobis; SCSE, Single-Cell Signature Explorer; ssGSEA, single sample Gene Set Enrichment Analysis.

Notably, numerous members of the CCT family (CCT2, CCT3, CCT5 and CCT6A) were consistently identified, suggesting that the CCT family may serve a broader and coordinated role in cisplatin resistance. Among these, CCT2 exhibited the most significant prognostic association, as it exhibited the smallest log-rank P-value in Kaplan-Meier survival analysis (Fig. 5C) and patients with high CCT2 expression demonstrated significantly worse overall survival, which led it to be prioritized for further investigation.

Single-cell transcriptomic profiling reveals the cell type-specific distribution and cisplatin resistance enrichment of core genes. Single-cell RNA-seq data from lung cancer samples retrieved from the GEO database (GSE229253) were used to explore the cellular origin and functional heterogeneity of the core genes at single-cell resolution. Dimensional reduction and clustering revealed key cell populations, including epithelial cells, macrophages, endothelial cells, T cells and B cells (Fig. 6A), with representative marker genes for each lineage displayed in Fig. 6B. Cell-cell communication networks inferred using CellChat revealed extensive intercellular interactions across these cell types (Fig. 6C). Visualization of core gene expression across cell populations demonstrated that CCT2, CCT3, CCT5 and CCT6A were predominantly enriched in epithelial cells (Fig. 6D). Further reclustering of epithelial cells revealed six distinct epithelial cell subpopulations, each characterized

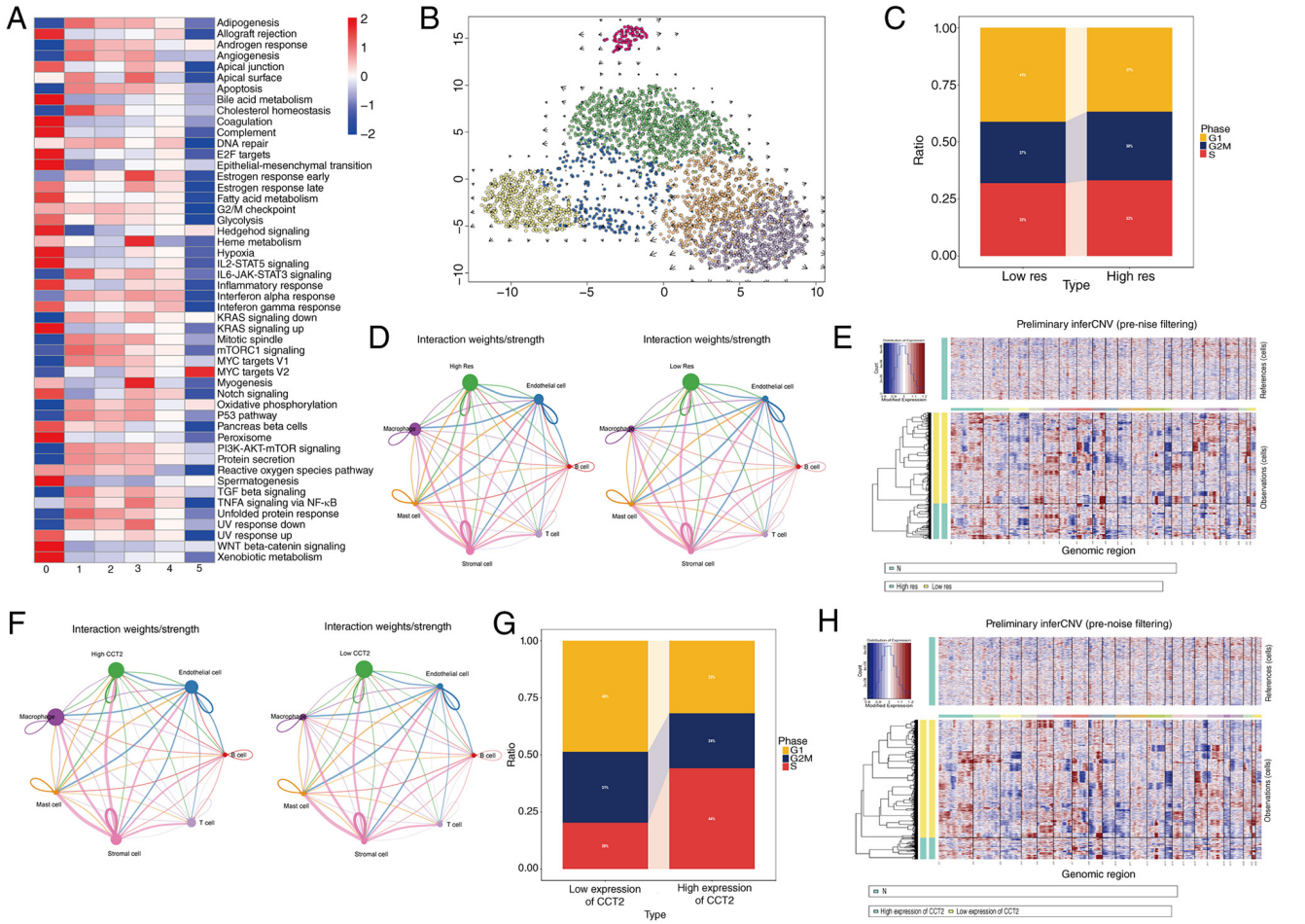

Figure 7. Single-cell functional characterization of CCT2 in epithelial subclusters. (A) Gene Set Variation Analysis showing pathway enrichment across six epithelial subclusters, with subcluster 0 enriched in oncogenic and proliferative pathways. (B) RNA velocity analysis indicating directional transcriptional flow from subcluster 0 to other epithelial subclusters. (C) Cell cycle phase distribution between high- and low-cisplatin-resistant epithelial cells. (D) Comparison of cell-cell communication intensity between resistance groups. (E) CNV profiles of epithelial cells stratified by cisplatin resistance status. (F) Cell-cell interaction strength in epithelial cells with high vs. low CCT2 expression. (G) Cell cycle phase distribution according to the CCT2 expression level. (H) CNV profiles comparing the high- and low-CCT2 epithelial subgroups. Res, cisplatin resistance; CNV, copy number variation; CCT, chaperonin-containing TCP-1.

by unique marker gene signatures (Fig. 6F). According to the results of the IRGSEA for resistance gene-set enrichment, subclusters 0 and 5 exhibited strong enrichment for cisplatin resistance signatures across numerous algorithms (Fig. 6G). Finally, mapping the five core genes onto epithelial subclusters demonstrated that CCT2, CCT3, CCT5 and CCT6A were significantly enriched in both cisplatin-resistant subclusters 0 and 5, whereas CENPK expression was predominantly enriched in subcluster 5 (Fig. 6H). These findings highlighted specific epithelial cell subpopulations as the principal cellular reservoirs of cisplatin resistance-associated gene activation.

Single-cell functional characterization of CCT2 in epithelial subclusters. GSVA across six epithelial subclusters revealed distinct biological functions of CCT2, with subcluster 0 exhibiting significant enrichment of genes associated with oncogenic and proliferative pathways, including genes associated with 'KRAS signaling up', 'Wnt beta-catenin signaling' and 'cell cycle' (Figs. 7A and S1). RNA velocity analysis further demonstrated a directional flow from subcluster 0 toward other epithelial subclusters, suggesting that subcluster 0 may represent a transcriptionally active and developmental origin state (Fig. 7B). On the basis of the IRGSEA-derived drug resistance signatures, the epithelial cells were stratified into high- and low-resistance groups. Cell cycle phase scoring indicated that, compared with the low-resistance group, the high-resistance group exhibited a markedly higher proportion of proliferating cells (S and G_2/M phases; Fig. 7C). Cell-cell communication analysis revealed that the high-resistance epithelial cell population exhibited stronger interactions with endothelial cells and mast cells compared with the low-resistance population, as indicated by the increased interaction strength in the communication network (Fig. 7D). Consistently, ligand-receptor analysis identified a greater number of significant interactions between these cell populations, including representative ligand-receptor pairs such as semaphorin-3C (SEMA3C)-[neuropilin (NRP)-2 + plexin-A2 (PLXNA2)], SEMA3C-(NRP1 + PLXNA2), SEMA3C-(NRP1 + NRP2), cell adhesion molecule 1 (CADM1)-CADM1 and amphiregulin (AREG)-EGFR, among others (Fig. S2). CNV profiling further demonstrated increased chromosomal instability in the resistant epithelial population (Fig. 7E). To clarify the contribution of CCT2 expression, epithelial cells were separately analyzed according to their CCT2 expression level. High-CCT2

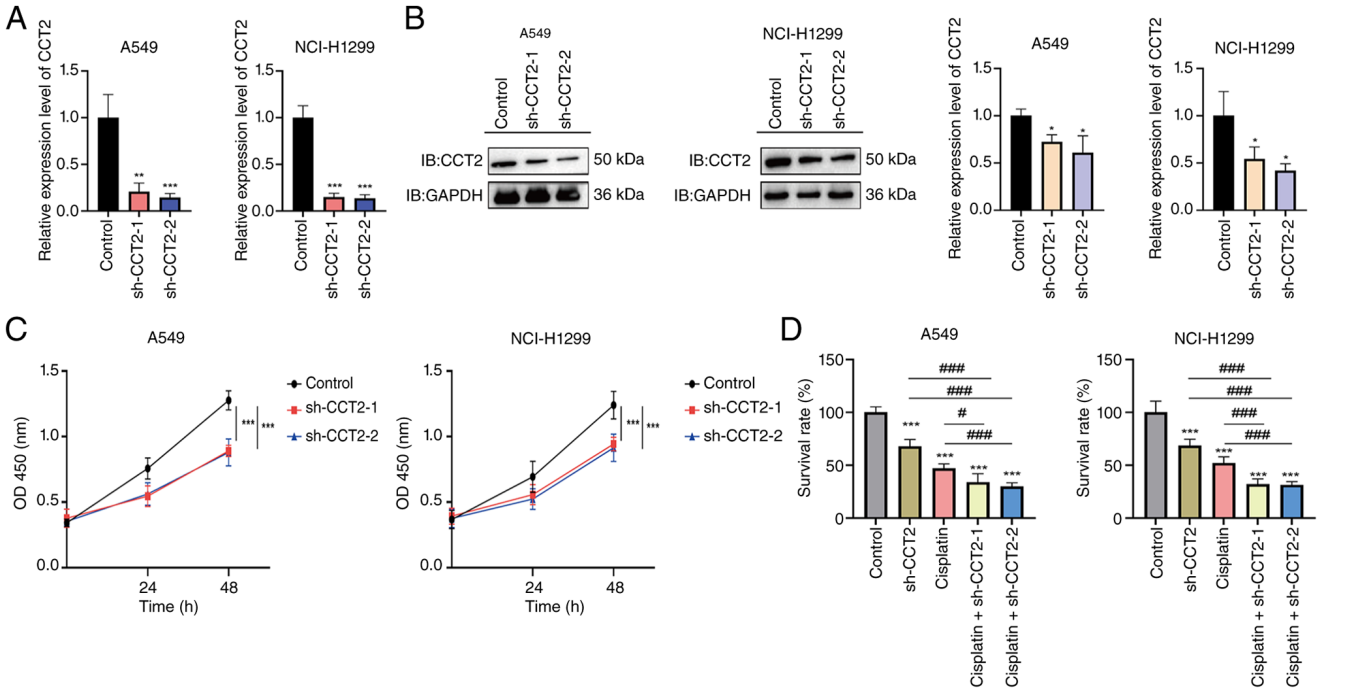

Figure 8. Experimental validation of the function of CCT2 in cisplatin resistance in lung cancer cells. (A) Quantitative PCR validation of the knockdown efficiency of CCT2 in A549 and H1299 cells transfected with shRNA expression vectors targeting CCT2. (B) Western blotting determination of CCT2 protein depletion following transfection with shRNA expression vectors targeting CCT2. (C) Cell Counting Kit-8 assays showing reduced cell proliferation after CCT2 silencing. (D) Cell viability under cisplatin treatment with or without CCT2 knockdown, indicating enhanced cisplatin sensitivity upon CCT2 depletion. Data are presented as the mean ± SD from at least three independent biological replicates. Statistical analysis for (A) and (B) were performed using one-way ANOVAs followed by Dunnett's multiple comparisons test, with all treatment groups compared to the control group. For (C), statistical significance was determined using two-way ANOVAs followed by Šidák's multiple comparisons test. For (D), statistical analysis was performed using a one-way ANOVA followed by Tukey's multiple comparisons test. *P<0.05, **P<0.01, ***P<0.001 vs. the control group; $^{\#}$P<0.05 and $^{\#\#\#}$P<0.001 indicate the comparisons between the indicated groups, as shown by the horizontal lines. ns, not significant; IB, immunoblotting; sh-, short hairpin; CCT, chaperonin-containing TCP-1; OD, optical density.

epithelial cells exhibited stronger interactions with endothelial cells and mast cells compared with low-CCT2 epithelial cells, as indicated by increased interaction strength in the communication network (Fig. 7F). Consistently, ligand-receptor analysis revealed a greater number of significant interactions between high-CCT2 epithelial cells and these cell populations, including representative ligand-receptor pairs such as SEMA3C-(NRP1 + PLXNA2), SEMA3C-(NRP1 + NRP2), secretoglobin family 3A member 2-macrophage receptor with collagenous structure, CADM1-CADM1 and AREG-EGFR, among others (Fig. S3). Consistent with the resistance-associated cell population, CCT2-high epithelial cells also exhibited a higher proportion of proliferating cells (S and G_2/M phases; Fig. 7G). In addition, CNV analysis showed greater genomic alterations in the high-CCT2 subgroup (Fig. 7H), collectively indicating that CCT2 upregulation was associated with proliferative activity, enhanced cellular communication and genomic instability within epithelial tumor cells.

Experimental validation of CCT2 function in cisplatin resistance. Functional roles of CCT2 were next validated in the cell lines A549 and NCI-H1299, respectively. A total of two shRNA expression constructs targeting CCT2 were transfected into both cell lines and qPCR determined the efficient knockdown by sh-CCT2-1 and sh-CCT2-2 (Fig. 8A; n=3; P<0.05). Western blotting analysis demonstrated that CCT2-targeting shRNA vectors effectively reduced CCT2 protein expression in A549 and NCI-H1299 cells (Fig. 8B; n=3; P<0.05). Cell proliferation assessed by CCK-8 assays at 24 and 48 h revealed that CCT2 depletion significantly reduced the proliferative capacity of both A549 and NCI-H1299 cells (Fig. 8C; n=5; P<0.05). To further evaluate whether CCT2 influences the cellular response to cisplatin, cells were treated with cisplatin following CCT2 knockdown. Cisplatin alone significantly suppressed cell viability, whereas combined treatment with cisplatin and CCT2 silencing resulted in a notably greater reduction in cell viability (Fig. 8D; n=5; P<0.05). Compared with cisplatin treatment alone, CCT2 knockdown further enhanced the inhibitory effect of cisplatin on cell viability, indicating that depletion of CCT2 increased the sensitivity of lung cancer cells to cisplatin. These findings indicated that CCT2 promoted lung cancer cell proliferation and modulated the sensitivity of lung cancer cells to cisplatin.

Identification of potential therapeutic compounds targeting CCT2. Molecular docking was performed using a natural-product compound library within the MOE platform to identify potential inhibitors of CCT2. A number of compounds, including deslanoside (-11.9 kcal/mol; Fig. 9A), digitoxin (-10.7 kcal/mol; Fig. 9B), lanatoside C (-11.8 kcal/mol; Fig. 9C), lecithin (-11.7 kcal/mol; Fig. 9D) and thymopentin (-10.9 kcal/mol; Fig. 9E), demonstrated strong binding affinities. Subsequent molecular dynamics simulations revealed stable RMSD, radius of gyration and solvent-accessible surface

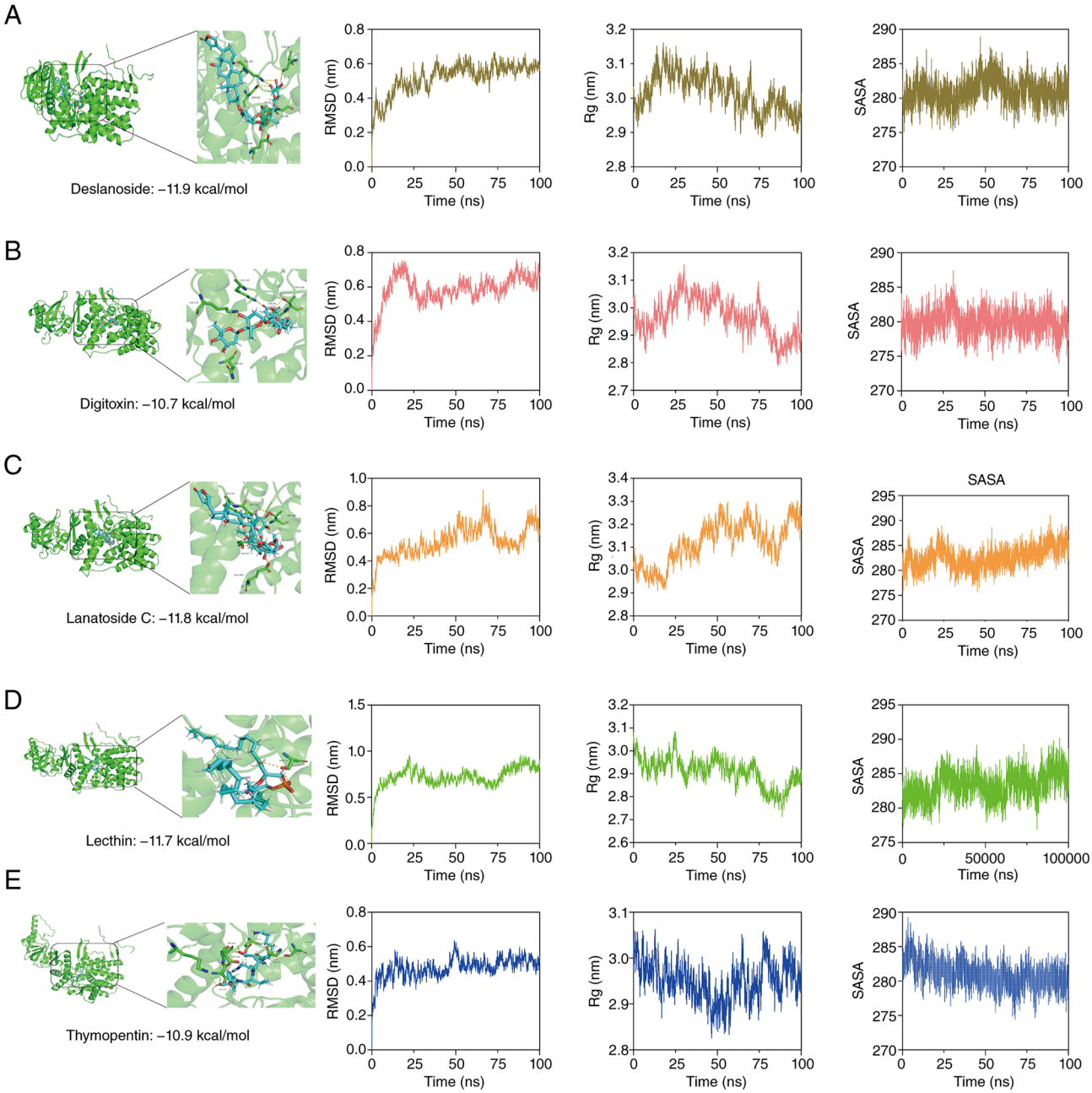

Figure 9. Identification of potential therapeutic compounds targeting CCT2. (A) Deslanoside, (B) digitoxin, (C) lanatoside C, (D) lecithin and (E) thymopentin. Molecular docking conformations and corresponding molecular dynamics simulation results with CCT2, including RMSD, Rg and SASA, indicating stable ligand-CCT2 interactions. CCT, chaperonin-containing TCP-1; RMSD, root mean square deviation; Rg, radius of gyration; SASA, solvent-accessible surface area.

area profiles for each ligand-protein complex, indicating stable binding conformations. These results suggested that the identified compounds may serve as promising candidates for targeting CCT2 in future therapeutic development.

Discussion

Despite marked advances in the treatment of LUAD, including targeted therapies, immunotherapy and emerging metabolism-oriented strategies, cisplatin-based chemotherapy remains a cornerstone of clinical management, particularly for patients without actionable driver mutations or those who are refractory to targeted and immunotherapeutic approaches (65-69). Although cisplatin-based chemotherapy provides substantial clinical benefit, its efficacy is often constrained by the development of adaptive resistance, including the emergence of resistant tumor cell populations with enhanced DNA damage repair capacity and altered apoptotic responses following cisplatin exposure (70,71). In particular, the efficacy of cisplatin is frequently undermined by the rapid development of acquired resistance, which is associated with alterations in DNA damage responses, cell cycle control, metabolic reprogramming and the tumor microenvironment (72-74). In routine clinical practice, the management of cisplatin resistance still relies largely on empirical combination therapies or treatment switching rather than mechanism-driven interventions, reflecting the lack of

robust molecular markers and validated therapeutic targets specific to cisplatin resistance in LUAD. Collectively, these difficulties underscore the need to systematically elucidate the molecular and cellular basis of cisplatin resistance to develop more precise and durable therapeutic strategies.

In the context of the clinical challenge of overcoming cisplatin resistance in LUAD, previous efforts have focused on identifying molecular determinants that underlie differential treatment responses. A number of genes and pathways, including TP53 signaling, cell cycle regulators and glycolytic pathways, have been implicated, yet their prognostic and therapeutic relevance remains unclear across cohorts (75-77). The present study systematically integrated bulk and single-cell transcriptomic data to define cisplatin resistance-associated molecular subtypes in LUAD. The present findings not only corroborate the enrichment of cell cycle- and DNA repair-associated pathways in resistant tumors but also reveal distinct immune infiltration patterns and notable cellular heterogeneity associated with resistance phenotypes. Notably, through machine learning-based feature selection, a robust core gene signature with both prognostic relevance and biological relevance was refined, offering a complementary approach to previous studies and enabling more comprehensive candidate gene identification and prognostic evaluation (78-80).

Notably, the present study highlights the CCT gene family, particularly CCT2, as key regulators of cisplatin resistance. The chaperonin-containing TCP-1 (CCT/TRiC) complex is essential for protein folding, cytoskeletal organization and cell cycle control, processes that are closely associated with tumor cell proliferation and stress adaptation (81-83). Emerging evidence has suggested that posttranslational modifications, including palmitoylation, modulate protein stability and signaling dynamics in cancer cells (84). By integrating palmitoylation-associated genes obtained from the GeneCards database with the present cisplatin resistance-associated gene sets, CCT2 was identified as a candidate gene of interest. In the present study, CCT2 was predominantly enriched in cisplatin-resistant epithelial cell subpopulation. In addition, CCT2-high epithelial cells exhibited a higher proportion of proliferating cells (S and G_2/M phases) and stronger interactions with endothelial cells and mast cells compared with CCT2-low epithelial cells, as indicated by increased communication strength in the network analysis and a greater number of ligand-receptor interactions/Functional validation further demonstrated that CCT2 knockdown enhanced the inhibitory effect of cisplatin on cell viability, suggesting that CCT2 depletion sensitizes lung cancer cells to cisplatin. Based on previous studies demonstrating the involvement of CCT2 in chaperonin-mediated protein folding and cell cycle regulation (85,86), it was speculated that CCT2 may contribute to cisplatin resistance by promoting tumor cell adaptation to chemotherapeutic stress. Previous studies have demonstrated that dysregulated G_2/M checkpoint progression and chaperonin-mediated proteostasis contribute notably to cisplatin resistance and tumor stress adaptation (87,88). In ovarian cancer, anlotinib reversed cisplatin resistance by inducing G_2/M arrest and apoptosis through the aurora kinase A/p53 pathway, highlighting the importance of cell cycle dysregulation in platinum resistance (87). In addition, CCT3 was upregulated in cisplatin-resistant LUAD cells, whereas CCT3 knockdown induced G_2/M arrest and apoptosis and restored cisplatin sensitivity through inhibition of the JAK2/STAT3 pathway (88).

In summary, the present study provides a comprehensive framework for understanding cisplatin resistance in LUAD through the integration of molecular subtyping, immune profiling, machine learning and experimental validation. The identification of CCT2 as a key resistance-associated gene offers new insights into the role of chaperonin-mediated regulation in chemotherapy resistance. Despite this, a number of limitations should be acknowledged. First, although the present integrative analyses and experimental validation suggest that CCT2 is associated with cisplatin resistance, the precise molecular mechanisms underlying its function, particularly its roles in protein folding and cell cycle regulation, require further in-depth investigation. Notably, future studies should include pathway-specific functional assays to directly determine whether CCT2 regulates these BPs. In addition, future studies should include CCT2 overexpression and rescue experiments (such as CCT2 re-expression following knockdown) to further establish the causal role of CCT2 in cisplatin resistance and determine whether CCT2 overexpression attenuates cisplatin-induced growth inhibition. Second, the present study was primarily based on public datasets and *in vitro* experiments and thus lacks validation in large-scale clinical cohorts and *in vivo* models. Therefore, the clinical predictive value and therapeutic potential of CCT2 need to be further determined in prospective studies. Third, although potential compounds targeting CCT2 have been identified through molecular docking, their biological efficacy and safety remain to be experimentally validated. Collectively, the present study provides a foundation for future mechanistic and translational studies aimed at overcoming cisplatin resistance in LUAD.

In conclusion, the present study systematically elucidated the molecular landscape of cisplatin resistance in LUAD through integrated multiomics analyses, machine learning-based modeling and experimental validation. A total of two distinct cisplatin resistance-associated molecular subtypes with significantly different prognoses, immune infiltration patterns and genomic alteration profiles were identified. By combining differential expression analysis, WGCNA, palmitoylation-associated gene sets and large-scale machine learning screening, the present study established a robust five-gene signature and highlighted CCT2 as a key regulator of cisplatin resistance. Single-cell analyses further revealed that CCT2 is preferentially enriched in resistant epithelial cell subpopulations and is associated with enhanced cell cycle activity, increased intercellular communication and genomic instability. Functional assays demonstrated that CCT2 knockdown significantly suppressed tumor cell proliferation and sensitized LUAD cells to cisplatin treatment. In addition, molecular docking and molecular dynamics simulations revealed a number of candidate compounds with stable binding to CCT2, suggesting potential therapeutic avenues. Collectively, the present findings provide novel insights into the mechanisms underlying cisplatin resistance in LUAD and identified CCT2 as a promising biomarker and therapeutic target, thereby offering a potential strategy for improving treatment efficacy and patient outcomes.

Acknowledgements

Not applicable.

Funding

No funding was received.

Availability of data and materials

The data generated in the present study may be requested from the corresponding author.

Authors' contributions

HM was responsible for study conceptualization, methodology, bioinformatics analysis, data curation, figure preparation and visualization and writing the original manuscript draft. CS was responsible for software implementation, computational analysis and interpretation of the data, validation of analytical results, investigation, and writing, reviewing and editing the manuscript. XH contributed to study conceptualization, interpretation of the data, scientific supervision, and writing, reviewing and editing the manuscript. GW was responsible for study conceptualization, funding acquisition, providing supervision and writing, reviewing and editing the manuscript. HM and GW confirm the authenticity of all the raw data. All authors read and approved the final version of the manuscript.

Ethics approval and consent to participate

Not applicable.

Patient consent for publication

Not applicable.

Competing interests

The authors declare that they have no competing interests.

References

1. Mangang KN and Rao G: Lung cancer biomarkers. Clin Chim Acta 580: 120707, 2026.
2. Ma J, Li S, Zhang X, Zhao P, Zhao B, Yue J, Han L, Bai J, Zhao Z and Zhang Y: Lung cancer organoids in translational research: Bridging basic science, drug development, and clinical therapeutics. Crit Rev Oncol Hematol 214: 104840, 2025.
3. Wang Y, Xu M, Wei X, Huang H, Chen Q, Chen B, Bao X and Li J: Prospective proteomics for discovering biomarkers in lung adenocarcinoma: A literature review. Transl Cancer Res 14: 6102-6117, 2025.
4. Sung H, Filho AM, Laversanne M, Ferlay J, Siegel RL, Soerjomataram I, Jemal A and Bray F: Global cancer statistics 2024: GLOBOCAN estimates of incidence and mortality worldwide for 34 cancers in 186 countries. CA Cancer J Clin 76: e70090, 2026.
5. Vokes NI, Pan K and Le X: Efficacy of immunotherapy in oncogene-driven non-small-cell lung cancer. Ther Adv Med Oncol 15: 17588359231161409, 2023.
6. Turcott JG, Cárdenas-Fernández D, Sánchez-Lara K, Palomares-Palomares CB and Arrieta O: Nutritional approach on management of diarrhea induced by EGFR-TKI's in advanced Non-Small cell lung cancer patients. Nutr Cancer 77: 567-574, 2025.
7. Ricco G, Seminerio R, Andrini E, Malvi D, Gruppioni E, Altimari A, Zagnoni S, Campana D and Lamberti G: BRAF V600E-mutated large cell neuroendocrine carcinoma responding to targeted therapy: A case report and review of the literature. Anticancer Drugs 34: 1076-1084, 2023.
8. Groehler A IV, Maratova A, Dao NM, Mahkmut A and Schärer OD: Development of comprehensive ultraperformance liquid Chromatography-High-Resolution mass spectrometry assays to quantitate Cisplatin-Induced DNA-DNA Cross-links. Chem Res Toxicol 36: 822-837, 2023.
9. Chen YF, Pang YC, Wang HC, Wu PE, Chen ZJ, Huang D, Peng DL, Yan YM, Liu C, Wu LC, *et al*: Identification of arnicolide C as a novel chemosensitizer to suppress mTOR/E2F1/FANCD2 axis in non-small cell lung cancer. Br J Pharmacol 181: 1221-1237, 2024.
10. Kuang L, Wang P, Zhou L and Li Y: Transformation of lung adenocarcinoma to small cell lung cancer following osimertinib treatment: A case report and literature review. Anticancer Drugs 36: 253-259, 2025.
11. Fennell DA, Summers Y, Cadranel J, Benepal T, Christoph DC, Lal R, Das M, Maxwell F, Visseren-Grul C and Ferry D: Cisplatin in the modern era: The backbone of first-line chemotherapy for non-small cell lung cancer. Cancer Treat Rev 44: 42-50, 2016.
12. Zhao Y, Zhang L, Xia L, E H, Wang T, Lu H, Chen H, She Y, Tang H, Wu J, *et al*: A METTL3-NFE2L3 axis mediates tumor stemness and progression in lung adenocarcinoma. Sci Adv 11: eadt7682, 2025.
13. Park JH, You GL, Ahn MJ, Kim SW, Hong MH, Han JY, Ock CY, Lee JS, Oh IJ, Lee SY, *et al*: Real-world outcomes of anti-PD1 antibodies in platinum-refractory, PD-L1-positive recurrent and/or metastatic non-small cell lung cancer, and its potential practical predictors: First report from Korean cancer study group LU19-05. J Cancer Res Clin Oncol 147: 2459-2469, 2021.
14. Liang J, Bi G, Huang Y, Zhao G, Sui Q, Zhang H, Bian Y, Yin J, Wang Q, Chen Z and Zhan C: MAFF confers vulnerability to cisplatin-based and ionizing radiation treatments by modulating ferroptosis and cell cycle progression in lung adenocarcinoma. Drug Resist Updat 73: 101057, 2024.
15. Jiang F, Shen Q, Zhang F, Fu J, Hu L, Wang J, Zhou H, Chen J and Wang Y: ADH1C facilitates cisplatin resistance of lung adenocarcinoma cells. DNA Cell Biol 41: 631-640, 2022.
16. Huang L, Lou K, Wang K, Liang L, Chen Y and Zhang J: Let-7c-5p represses cisplatin resistance of lung adenocarcinoma cells by targeting CDC25A. Appl Biochem Biotechnol 195: 1644-1655, 2023.
17. Kiss RC, Xia F and Acklin S: Targeting DNA damage response and repair to enhance therapeutic index in Cisplatin-Based cancer treatment. Int J Mol Sci 22: 8199, 2021.
18. Qiao X, Li W, Zheng Z, Liu C, Zhao L, He Y and Li H: Inhibition of the HMGB1/RAGE axis protects against cisplatin-induced ototoxicity via suppression of inflammation and oxidative stress. Int J Biol Sci 20: 784-800, 2024.
19. Cai L, Zhang Q, Du L and Zheng F: Silencing of miR-1246 induces cell cycle arrest and apoptosis in Cisplatin-Resistant ovarian cancer cells by promoting ZNF23 transcription. Cytogenet Genome Res 161: 488-500, 2021.
20. Haroon M and Kang SC: Kaempferol synergistically enhances Cisplatin-induced apoptosis and cell cycle arrest in colon cancer cells. J Cancer Prev 29: 69-87, 2024.
21. Rao L, Guo D and Wu JP: Cisplatin-resistance induces lung squamous carcinoma cell growth by nicotine-mediated α7nAchR/HDAC1/Cyclin D1/pRb cell cycle activation. Cell Biochem Funct 42: e3990, 2024.
22. Xie R, Cheng L, Huang M, Huang L, Chen Z, Zhang Q, Li H, Lu J, Wang H, Zhou Q, *et al*: NAT10 drives cisplatin chemoresistance by enhancing ac4C-Associated DNA repair in bladder cancer. Cancer Res 83: 1666-1683, 2023.
23. Ye W, Fan C, Fu K, Wang X, Lin J, Nian S, Liu C and Zhou W: The SAR and action mechanisms of autophagy inhibitors that eliminate drug resistance. Eur J Med Chem 244: 114846, 2022.
24. Yang L, Xie HJ, Li YY, Wang X, Liu XX and Mai J: Molecular mechanisms of platinum-based chemotherapy resistance in ovarian cancer (Review). Oncol Rep 47: 82, 2022.
25. Laurino S, Mazzone P, Ruggieri V, Zoppoli P, Calice G, Lapenta A, Ciuffi M, Ignomirelli O, Vita G, Sgambato A, *et al*: Cationic channel TRPV2 overexpression promotes resistance to Cisplatin-induced apoptosis in gastric cancer cells. Front Pharmacol 12: 746628, 2021.
26. Wang D, Zhao C, Xu F, Zhang A, Jin M, Zhang K, Liu L, Hua Q, Zhao J, Liu J, *et al*: Cisplatin-resistant NSCLC cells induced by hypoxia transmit resistance to sensitive cells through exosomal PKM2. Theranostics 11: 2860-2875, 2021.

27. Miao C, Huang Y, Zhang C, Wang X, Wang B, Zhou X, Song Y, Wu P, Chen ZS and Feng Y: Post-translational modifications in drug resistance. Drug Resist Updat 78: 101173, 2025.
28. Arora G, Bothra A, Prosser G, Arora K and Sajid A: Role of post-translational modifications in the acquisition of drug resistance in Mycobacterium tuberculosis. FEBS J 288: 3375-3393, 2021.
29. Hu S, Xu J, Cui W, Jin H, Wang X and Maimaitiyiming Y: Post-translational modifications in multiple myeloma: Mechanisms of drug resistance and therapeutic opportunities. Biomolecules 15: 702, 2025.
30. Jin J, Zhi X, Wang X and Meng D: Protein palmitoylation and its pathophysiological relevance. J Cell Physiol 236: 3220-3233, 2021.
31. He Q, Qu M, Shen T, Su J, Xu Y, Xu C, Barkat MQ, Cai J, Zhu H, Zeng LH and Wu X: Control of mitochondria-associated endoplasmic reticulum membranes by protein S-palmitoylation: Novel therapeutic targets for neurodegenerative diseases. Ageing Res Rev 87: 101920, 2023.
32. He Y, Li S, Jiang L, Wu K, Chen S, Su L, Liu C, Liu P, Luo W, Zhong S and Li Z: Palmitic acid accelerates endothelial cell injury and cardiovascular dysfunction via palmitoylation of PKM2. Adv Sci (Weinh) 12: e2412895, 2025.
33. Zhang H, Sun Y, Wang Z, Huang X, Tang L, Jiang K and Jin X: ZDHHC20-mediated S-palmitoylation of YTHDF3 stabilizes MYC mRNA to promote pancreatic cancer progression. Nat Commun 15: 4642, 2024.
34. Liu Z, Xiao M, Mo Y, Wang H, Han Y, Zhao X, Yang X, Liu Z and Xu B: Emerging roles of protein palmitoylation and its modifying enzymes in cancer cell signal transduction and cancer therapy. Int J Biol Sci 18: 3447-3457, 2022.
35. Xu M, Zheng Y, Chen J, Gao C, Zhu M, Ma A, Liang B, Xu W, Fan J, Zhou H, *et al*: CLDN4 palmitoylation promotes hepatic-to-biliary lineage transition and lenvatinib resistance in hepatocellular carcinoma. Cell Rep Med 6: 102208, 2025.
36. Jeong DW, Park JW, Kim KS, Kim J, Huh J, Seo J, Kim YL, Cho JY, Lee KW, Fukuda J and Chun YS: Palmitoylation-driven PHF2 ubiquitination remodels lipid metabolism through the SREBP1c axis in hepatocellular carcinoma. Nat Commun 14: 6370, 2023.
37. Wang J, Li DL, Zheng LF, Ren S, Huang ZQ, Tao Y, Liu Z, Shang Y, Pang D, Guo H, *et al*: Dynamic palmitoylation of STX11 controls injury-induced fatty acid uptake to promote muscle regeneration. Dev Cell 59: 384-399.e5, 2024.
38. Teuber JP, Scissors RE, Subramani A, Madamanchi N and Brody MJ: Rac1 palmitoylation is required for cardiac stress adaptation and regulation of protein kinase A signaling. JCI Insight 10: e193733, 2025.
39. Chen X, Zhou Y, Zhang Z, Yuan G, He S and Xiao F: Identification of mitochondrial dysfunction-related biomarkers and immune infiltration in liver ischemia-reperfusion injury via integrated bioinformatics and machine learning. Biochem Biophys Res Commun 807: 153435, 2026.
40. Liu J, Shi Y and Zhang Y: Multi-omics identification of an immunogenic cell death-related signature for clear cell renal cell carcinoma in the context of 3P medicine and based on a 101-combination machine learning computational framework. EPMA J 14: 275-305, 2023.
41. Yu Y, Liu H, Liu K, Zhao M, Zhang Y, Jiang R and Wang F: Multi-omics identification of a polyamine metabolism related signature for hepatocellular carcinoma and revealing tumor microenvironment characteristics. Front Immunol 16: 1570378, 2025.
42. Chavez-Dominguez R, Aguilar-Cazares D, Perez-Medina M, Avila-Rios S, Soto-Nava M, Mendez-Tenorio A, Islas-Vazquez L, Benito-Lopez JJ, Galicia-Velasco M and Lopez-Gonzalez JS: Transcriptional signature of early cisplatin drug-tolerant persister cells in lung adenocarcinoma. Front Oncol 13: 1208403, 2023.
43. Dolgalev I, Zhou H, Murrell N, Le H, Sakellaropoulos T, Coudray N, Zhu K, Vasudevaraja V, Yeaton A, Goparaju C, *et al*: Inflammation in the tumor-adjacent lung as a predictor of clinical outcome in lung adenocarcinoma. Nat Commun 14: 6764, 2023.
44. Wilkerson MD and Hayes DN: ConsensusClusterPlus: A class discovery tool with confidence assessments and item tracking. Bioinformatics 26: 1572-1573, 2010.
45. Newman AM, Liu CL, Green MR, Gentles AJ, Feng W, Xu Y, Hoang CD, Diehn M and Alizadeh AA: Robust enumeration of cell subsets from tissue expression profiles. Nat Methods 12: 453-457, 2015.
46. Mayakonda A, Lin DC, Assenov Y, Plass C and Koeffler HP: Maftools: Efficient and comprehensive analysis of somatic variants in cancer. Genome Res 28: 1747-1756, 2018.
47. Ritchie ME, Phipson B, Wu D, Hu Y, Law CW, Shi W and Smyth GK: Limma powers differential expression analyses for RNA-sequencing and microarray studies. Nucleic Acids Res 43: e47, 2015.
48. Langfelder P and Horvath S: WGCNA: An R package for weighted correlation network analysis. BMC Bioinformatics 9: 559, 2008.
49. Gene Ontology Consortium: The Gene Ontology resource: Enriching a GOld mine. Nucleic Acids Res 49: D325-D334, 2021.
50. Kanehisa M, Furumichi M, Sato Y, Kawashima M and Ishiguro-Watanabe M: KEGG for taxonomy-based analysis of pathways and genomes. Nucleic Acids Res 51: D587-D592, 2023.
51. Wu T, Hu E, Xu S, Chen M, Guo P, Dai Z, Feng T, Zhou L, Tang W, Zhan L, *et al*: clusterProfiler 4.0: A universal enrichment tool for interpreting omics data. Innovation (Camb) 2: 100141, 2021.
52. Hänzelmann S, Castelo R and Guinney J: GSVA: Gene set variation analysis for microarray and RNA-seq data. BMC Bioinformatics 14: 7, 2013.
53. Jan B, Kosztyla D, von Törne C, *et al*: cancerclass: An R Package for development and validation of diagnostic tests from high-dimensional molecular data. J Statist Software 59: 1-19, 2014.
54. Rohart F, Gautier B, Singh A and Lê Cao KA: mixOmics: An R package for 'omics feature selection and multiple data integration. PLoS Comput Biol 13: e1005752, 2017.
55. Leek JT and Storey JD: Capturing heterogeneity in gene expression studies by surrogate variable analysis. PLoS Genet 3: 1724-1735, 2007.
56. Gu Z, Eils R and Schlesner M: Complex heatmaps reveal patterns and correlations in multidimensional genomic data. Bioinformatics 32: 2847-2849, 2016.
57. Binder H and Schumacher M: Allowing for mandatory covariates in boosting estimation of sparse high-dimensional survival models. BMC Bioinformatics 9: 14, 2008.
58. Liu H, Zhang W, Zhang Y, Adegboro AA, Fasoranti DO, Dai L, Pan Z, Liu H, Xiong Y, Li W, *et al*: Mime: A flexible machine-learning framework to construct and visualize models for clinical characteristics prediction and feature selection. Comput Struct Biotechnol J 23: 2798-2810, 2024.
59. Hao Y, Hao S, Andersen-Nissen E, Mauck WM III, Zheng S, Butler A, Lee MJ, Wilk AJ, Darby C, Zager M, *et al*: Integrated analysis of multimodal single-cell data. Cell 184: 3573-3587.e29, 2021.
60. Aran D, Looney AP, Liu L, Wu E, Fong V, Hsu A, Chak S, Naikawadi RP, Wolters PJ, Abate AR, *et al*: Reference-based analysis of lung single-cell sequencing reveals a transitional profibrotic macrophage. Nat Immunol 20: 163-172, 2019.
61. Jin S, Guerrero-Juarez CF, Zhang L, Chang I, Ramos R, Kuan CH, Myung P, Plikus MV and Nie Q: Inference and analysis of cell-cell communication using CellChat. Nat Commun 12: 1088, 2021.
62. Patel AP, Tirosh I, Trombetta JJ, Shalek AK, Gillespie SM, Wakimoto H, Cahill DP, Nahed BV, Curry WT, Martuza RL, *et al*: Single-cell RNA-seq highlights intratumoral heterogeneity in primary glioblastoma. Science 344: 1396-1401, 2014.
63. Livak KJ and Schmittgen TD: Analysis of relative gene expression data using real-time quantitative PCR and the 2(-Delta Delta C(T)) method. Methods 25: 402-408, 2001.
64. Corbeil CR, Williams CI and Labute P: Variability in docking success rates due to dataset preparation. J Comput Aided Mol Des 26: 775-786, 2012.
65. Qin L, Cheng X, Wang S, Gong G, Su H, Huang H, Chen T, Damdinjav D, Dorjsuren B, Li Z, *et al*: Discovery of novel aminobutanoic Acid-Based ASCT2 inhibitors for the treatment of Non-Small-cell lung cancer. J Med Chem 67: 988-1007, 2024.
66. Tan AC and Tan DSW: Targeted therapies for lung cancer patients with oncogenic driver molecular alterations. J Clin Oncol 40: 611-625, 2022.
67. Lahiri A, Maji A, Potdar PD, Singh N, Parikh P, Bisht B, Mukherjee A and Paul MK: Lung cancer immunotherapy: Progress, pitfalls, and promises. Mol Cancer 22: 40, 2023.
68. Meyer ML, Fitzgerald BG, Paz-Ares L, Cappuzzo F, Jänne PA, Peters S and Hirsch FR: New promises and challenges in the treatment of advanced non-small-cell lung cancer. Lancet 404: 803-822, 2024.
69. Chaft JE, Shyr Y, Sepesi B and Forde PM: Preoperative and postoperative systemic therapy for operable Non-Small-Cell lung cancer. J Clin Oncol 40: 546-555, 2022.

70. Galluzzi L, Senovilla L, Vitale I, Michels J, Martins I, Kepp O, Castedo M and Kroemer G: Molecular mechanisms of cisplatin resistance. Oncogene 31: 1869-1883, 2012.
71. Amable L: Cisplatin resistance and opportunities for precision medicine. Pharmacol Res 106: 27-36, 2016.
72. Liu C, Pan S, Pan X, Yang J, Yao H, Yang Z, Hao S, Liu Y, Liu P and Zhang S: High-throughput single-cell metabolites profiling reveals metabolic reprogramming confers cisplatin resistance in lung cancer. Talanta 285: 127355, 2025.
73. Kryczka J, Kryczka J, Czarnecka-Chrebelska KH and Brzeziańska-Lasota E: Molecular mechanisms of chemoresistance induced by cisplatin in NSCLC cancer therapy. Int J Mol Sci 22: 8885, 2021.
74. Yu X, Jia L, Tang Q, Zhou Q, Wang G and Wang S: Regulation of cisplatin resistance in lung cancer by epigenetic mechanisms. Clin Epigenetics 17: 145, 2025.
75. Lin L, Zou Y and Zhang D: Silencing ribosome biogenesis regulator 1 homolog (RRS1) inhibits angiogenesis and cisplatin resistance of lung cancer cells by activating ferroptosis mediated by p53 pathway. Tissue Cell 94: 102796, 2025.
76. Jang M, Park R, Park YI, Park Y, Lee JI, Namkoong S, Lee EJ and Park J: LNX1 Contributes to cell cycle progression and cisplatin resistance. Cancers (Basel) 13: 4066, 2021.
77. Su P, Mao X, Ma J, Huang L, Yu L, Tang S, Zhuang M, Lu Z, Osafo KS, Ren Y, *et al*: ERRα promotes glycolytic metabolism and targets the NLRP3/caspase-1/GSDMD pathway to regulate pyroptosis in endometrial cancer. J Exp Clin Cancer Res 42: 274, 2023.
78. Lv M, Tang L, Yang L, Yu J, Ji Q and Zhao R: Identification and experimental verification of a novel cisplatin resistance-related lncRNA signature for predicting prognosis and immune response in lung adenocarcinoma. Clin Transl Oncol 28: 1178-1197, 2026.
79. Mao X, Xu S, Wang H, Xiao P, Li S, Wu J, Sun J, Jin C, Shen M, Shi Y, *et al*: Integrated analysis reveals critical cisplatin-resistance regulators E2F7 contributed to tumor progression and metastasis in lung adenocarcinoma. Cancer Cell Int 24: 173, 2024.
80. Yu H, Zhang W, Xu XR and Chen S: Drug resistance related genes in lung adenocarcinoma predict patient prognosis and influence the tumor microenvironment. Scientific reports 13: 9682, 2023.
81. Shen PS and Willardson BM: Protein folding by the CCT/TRiC chaperone complex. Curr Opin Struct Biol 91: 102999, 2025.
82. Wang DY, Kamuda K, Montoya G and Mesa P: The TRiC/CCT chaperonin and its role in uncontrolled proliferation. Adv Exp Med Biol 1243: 21-40, 2020.
83. Vallin J and Grantham J: The role of the molecular chaperone CCT in protein folding and mediation of cytoskeleton-associated processes: Implications for cancer cell biology. Cell Stress Chaperones 24: 17-27, 2019.
84. Ko PJ and Dixon SJ: Protein palmitoylation and cancer. EMBO Rep 19: e46666, 2018.
85. Ghozlan H, Showalter A, Lee E, Zhu X and Khaled AR: Chaperonin-containing TCP1 complex (CCT) promotes breast cancer growth through correlations with key cell cycle regulators. Front Oncol 11: 663877, 2021.
86. Zhao F, Yao Z, Li Y, Zhao W, Sun Y, Yang X, Zhao Z, Huang B, Wang J, Li X and Chen A: Targeting the molecular chaperone CCT2 inhibits GBM progression by influencing KRAS stability. Cancer Lett 590: 216844, 2024.
87. Wang H and Wang Y: Anlotinib induces apoptosis and second growth/mitosis phase block in cisplatin-resistant ovarian cancer cells via the aurora kinase A/p53 pathway. Hum Exp Toxicol 42: 9603271231185774, 2023.
88. Danni X, Jiangzheng Z, Huamao S, Yinglian P, Changcheng Y and Yanda L: Chaperonin containing TCP1 subunit 3 (CCT3) promotes cisplatin resistance of lung adenocarcinoma cells through targeting the Janus kinase 2/signal transducers and activators of transcription 3 (JAK2/STAT3) pathway. Bioengineered 12: 7335-7347, 2021.